Atmospheric Research 342 (2026) 109156

Contents lists available at ScienceDirect

Atmospheric Research

journal homepage: www.elsevier.com/locate/atmosres

The importance of mesoscale convective systems for summer lightning and rainfall over southern Africa

Ross C. Blamey [a,*], Mulalo Maphugwi [a], Cornelia Klein [b], Morne Gijben [c], Chris J.C. Reason [a]

[a] Department of Oceanography, University of Cape Town, South Africa
[b] UK Centre for Ecology and Hydrology, Wallingford, United Kingdom
[c] South African Weather Service, Centurion, South Africa

ARTICLE INFO

Keywords:
Mesoscale convective systems
Rainfall
Lightning
Climatology
El Niño-Southern Oscillation
Southern Africa

ABSTRACT

Mesoscale convective systems (MCSs) are large, long-lived thunderstorms that produce much of the rainfall in the tropics and subtropics, yet their role in southern African rainfall and lightning has remained poorly quantified. Using a 14-year (2010–2024) satellite-based MCS climatology derived with the PyFLEXTRKR tracking algorithm, we assess the seasonal and spatial contributions of MCSs to austral summer (October–March) rainfall and lightning across subtropical southern Africa. On average, MCSs account for over 30% of summer rainfall and more than 50% of cloud-to-ground lightning across eastern South Africa, eSwatini, southeast Zimbabwe, and southern Mozambique. There is a strong seasonal cycle in both MCS activity and rainfall contribution across southern Africa where these systems are most frequent and contribute the most during the early summer months (November and December). Parts of Zimbabwe and Mozambique, as well as the drier western half of southern Africa (Namibia, Botswana and central South Africa), show a significant relationship between interannual variability in MCS frequency, rainfall and the El Niño-Southern Oscillation. There is a clear sensitivity to calculating the MCS contribution to rainfall and lightning activity based on the criteria used to identify and track the systems. Nevertheless, results here underscore the critical role of MCSs in the southern Africa convective landscape as by being a key producer of both summer lightning and rainfall. With the added importance of this being that southern Africa is not only a water stressed region dependent on these convective storms for rainfall, but a domain with a population highly vulnerable to extreme weather events.

1. Introduction

Mesoscale convective systems (MCSs) are large, long-lived thunderstorm clusters that play a crucial role in the global water and energy cycles. They organise from ensembles of cumulonimbus towers into coherent structures that can span hundreds of kilometres and persist for many hours, producing extensive rainfall, lightning, and severe weather (Houze, 2004, 2018). Because of their longevity and organisation, MCSs are responsible for a large share of tropical and subtropical rainfall, reaching over 50% in many regions (Yuan and Houze, 2010; Feng et al., 2025; Rajagopal et al., 2023), with long-lived MCSs contributing disproportionately to rainfall extremes (Roca and Fiolleau, 2020). Outside the tropics, they make important contributions in subtropical and midlatitude zones such as the central United States and South America (Fritsch et al., 1986; Durkee et al., 2009; Ambrizzi and Rehbein, 2025). Their impacts extend beyond hydrology, including damaging winds, hail, flooding, and lightning, with major socio-economic consequences worldwide.

Despite this global importance, MCSs remain poorly characterised over much of Africa, particularly in the southern subtropics. Most African MCS lifecycle studies have focused on West and Central Africa (e.g. Mathon and Laurent, 2001; Crook et al., 2019; Andrews et al., 2024), while southern Africa has received less attention and is represented mainly by short climatologies or case studies (e.g., Blamey and Reason, 2009, 2012; Morake et al., 2021; van Schalkwyk et al., 2025). Yet this region is highly vulnerable to convective extremes: it is water-stressed, strongly dependent on summer rainfall, and experiences frequent flooding and lightning fatalities. Understanding how much of its rainfall and lightning arises from MCSs is therefore essential for managing both water resources and weather hazards.

Rainfall across southern Africa occurs mainly during the austral summer (October–March) and is predominantly convective, controlled

* Corresponding author at: Dept. of Oceanography, University of Cape Town, Private Bag X3, Rondebosch 7701, South Africa.
E-mail address: ross.blamey@uct.ac.za (R.C. Blamey).

https://doi.org/10.1016/j.atmosres.2026.109156
Received 3 February 2026; Received in revised form 1 June 2026; Accepted 11 June 2026
Available online 17 June 2026

by large-scale and regional circulations (Tyson and Preston-Whyte, 2000). The formation and intensification of the Angola and Kalahari heat lows in early summer weaken subtropical subsidence and promote convection (Munday and Washington, 2017). Interaction between these lows and midlatitude disturbances passing south of the continent draws moist tropical air poleward, producing northwest–southeast-oriented cloud bands that are major contributors to widespread rainfall (Harrison, 1984; Hart et al., 2013). Additional synoptic systems such as cut-off lows (Favre et al., 2012), ridging anticyclones (Ndarana et al., 2020) and occasional tropical cyclones (Malherbe et al., 2012) further modulate summer rainfall variability.

Embedded within these broader systems is a spectrum of convective organisation ranging from isolated thunderstorms to well-organised MCSs. The eastern half of southern Africa, encompassing eastern South Africa, eSwatini, southern Mozambique, and southeast Zimbabwe, is a regional hotspot for organised convection (Brooks et al., 2003; Zipser et al., 2006; Blamey et al., 2016; Hart et al., 2019; Mawren et al., 2023). Here, steep topography, strong land–sea contrasts, and proximity to the warm Agulhas Current (see Fig. 1) enhance storm development (Blamey and Reason, 2009). The elevated interior plateau that reaches 1–1.5 km in altitude is separated from a narrow coastal plain by the eastern escarpment, while the Agulhas Current provides a continuous supply of heat and moisture that fuels deep convection (Reason, 2001; Rouault et al., 2002). These factors combine to favour frequent, intense convective systems that often propagate eastwards from the eastern escarpment towards the coast.

Recent years have seen several destructive events linked to organised convection, including catastrophic flooding along the KwaZulu-Natal coast in April 2022 (Thoithi et al., 2023), an EF3 tornado near Durban in June 2024, and extensive floods in the Eastern Cape in May 2025.

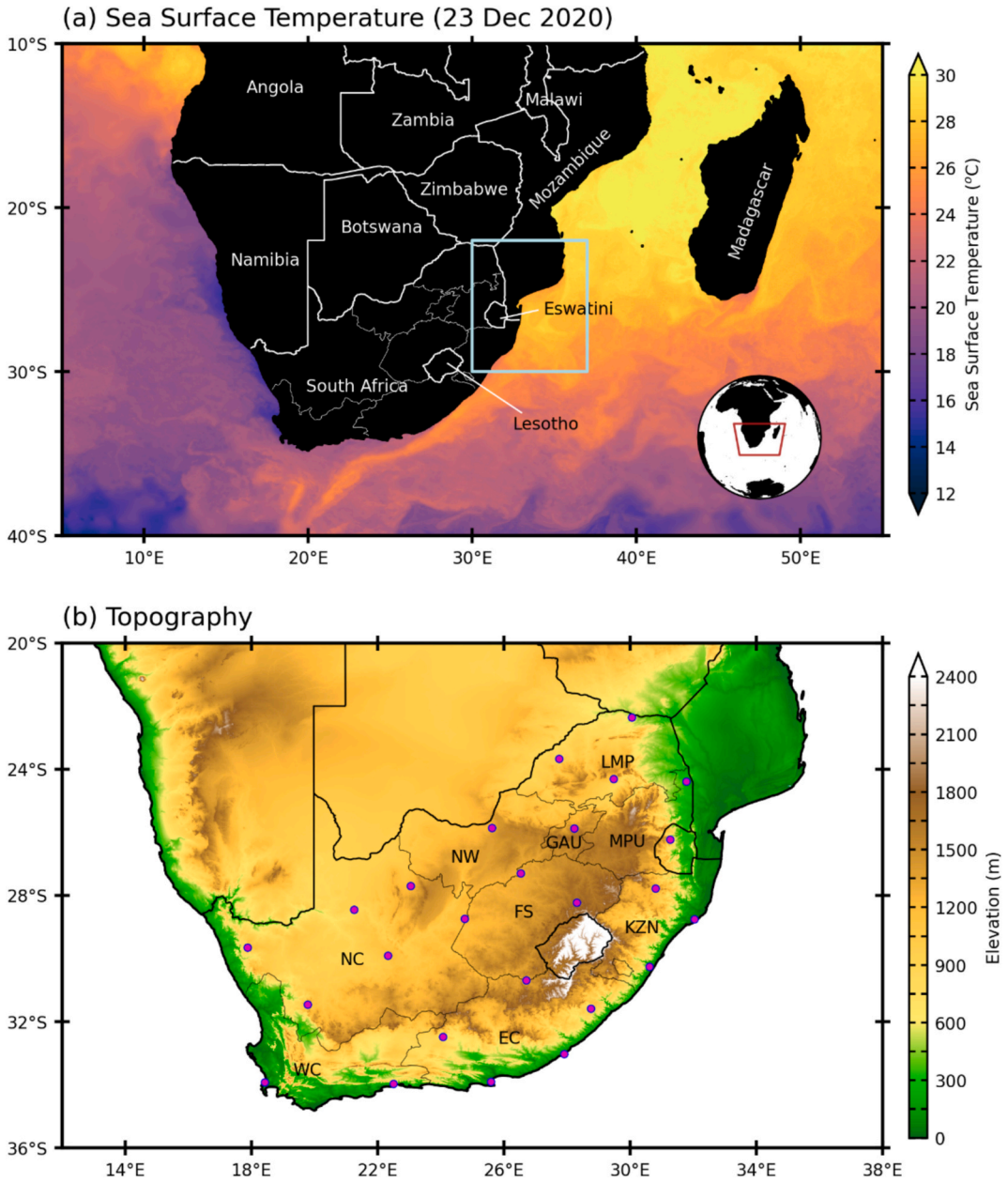

Fig. 1. (a) Snapshot of sea surface temperature (shaded; °C) on 23 December 2020 based on 0.01° horizontal resolution daily Multi-scale Ultra-high Resolution (MUR) SST data. (b) Topography (shaded; m) of southern Africa, with the location of the South African provinces which are commonly referred to in the text. KZN: KwaZulu-Natal, MP: Mpumalanga, LP: Limpopo, GAU: Gauteng, FS: Free State, NW: North-West, NC: Northern Cape and WC: Western Cape. Locations of SALDN sensors are indicated by purple circles. (For interpretation of the references to colour in this figure legend, the reader is referred to the web version of this article.)

Lightning alone causes around 100 deaths per year across South Africa (McCain, 2022), with fatality rates several times higher than in most developed countries (Gill, 2008; Holle, 2008). Such impacts emphasise the need for a clearer understanding of the convective systems that dominate the region's summer rainfall and lightning activity.

MCSs are particularly relevant in this context. Their organised structure enables repeated convective regeneration and extensive stratiform precipitation, giving them a much greater hydrological impact than isolated storms. However, quantitative information on their frequency, spatial distribution, and rainfall contribution across southern Africa is scarce. Previous studies have mainly examined individual events (e.g., Blamey and Reason, 2009; Mpungose et al., 2022; Thoithi et al., 2023) or limited domains and periods (e.g. Blamey and Reason, 2012). The only earlier regional estimate suggested that mesoscale convective complexes - the largest subset of MCSs - can contribute up to 20% of summer rainfall in eastern South Africa (Blamey and Reason, 2013), but this was based on a short record. Thus, the overall role of MCSs in producing rainfall and lightning across the broader southern African region remains largely unknown.

Recent advances in satellite observations and automated tracking algorithms have now made it possible to identify and follow MCSs consistently over long time periods. The Python FLEXible object TRacKeR (PyFLEXTRKR; Feng et al., 2019, 2021, 2023a) algorithm, which combines infrared brightness temperature (T_b) and precipitation data, has been widely used to develop global and regional MCS climatologies. A new southern Africa MCS database based on PyFLEXTRKR, including regional modifications to account for local storm characteristics, has recently been produced by Maphugwi (2026). This database provides, for the first time, a 14-year record (2010–2024) of objectively identified and tracked MCSs across subtropical southern Africa.

In this study, we use this new climatology to quantify the contribution of MCSs to austral-summer rainfall and lightning over southern Africa. Specifically, we (1) analyse the spatial and seasonal distribution of MCSs, (2) determine their fractional contribution to total rainfall and cloud-to-ground lightning activity, and (3) evaluate the sensitivity of these contributions to the thresholds used for MCS identification. The results provide a comprehensive assessment of the role of MCSs in the convective climate of southern Africa, clarifying their importance for both hydrological processes and weather-related hazards in a region that is simultaneously rainfall-dependent and highly vulnerable to extreme convective events.

2. Data and methodology

2.1. The MCS climatology

The MCS database used in this study is based on the work of Maphugwi (2026), which used a modified version of the Python FLEXible object TRacKeR (PyFLEXTRKR; Feng et al., 2019; Feng et al., 2021; Feng et al., 2023a) to identify and track MCSs. The PyFLEXTRKR software package is designed to identify and track MCS features using either brightness temperature (T_b) alone or a combination of T_b and precipitation, with the workflow outlined in Feng et al. (2023a). For brevity, the process begins with identification of a cold cloud shield (CCS) associated with a convective feature in the observational datasets (discussed below). Once individual CCS segments are identified, temporal linkage is established by associating CCSs from consecutive time steps (1 h apart) if they share more than 50% of their spatial area. A temporarily linked CSS track is classified as an MCS if the cloud shield area exceeds 40,000 km^2 and persists longer than 4 h. However, as noted by Maphugwi (2026), automated tracking of MCSs still has some challenges, which primarily revolves around the lack of any standardised MCS identification criteria and the inclusion of non-MCS precipitation systems. Therefore, based on a series of sensitivity tests, Maphugwi (2026) implemented some modifications of the original algorithm, which include:

i. *A colder "cold core" brightness temperature is used*: The brightness temperature used to identify / track MCSs in the original code identifies a cold cloud shield (CCS) by iteratively expanding a contiguous region from a cold cloud core, defined by $T_b < 225$ K (−48.15 °C), outward to an outer threshold of 241 K (−32.15 °C). In Maphugwi (2026), a slight modification is made where the CCS is detected by iteratively growing a cold core with $T_b < 221$ K (−52.15 °C) outwards to 235 K (−38.15 °C).

ii. *Only a single rainfall threshold is used:* There are two rainfall thresholds used in the original code, with that being a rain rate exceeding 2 $mm.hr^{-1}$ and one of 10 $mm.hr^{-1}$. In their sensitivity analysis, Maphugwi (2026) documented that the heavy rainfall requirement can pose a challenge for the identification and tracking of MCSs over southern Africa. This may be due to IMERG underestimating rainfall intensity in Africa (Amell et al., 2025). For this reason, the requirement of the system to have a rain rate > 10 $mm.hr^{-1}$ during part of the MCS life cycle is removed and makes the MCS detection less sensitive to IMERG underestimates in rainfall intensity.

iii. *Removal of frontal systems*: One of the challenges in MCS tracking in PyFLEXTRKR is when the methodology identifies and tracks other large precipitating cloud systems such as tropical cyclones (TCs) or strong cold fronts (Feng et al., 2021). Although cold fronts and associated extra-tropical cyclones typically pass to the south of the African continent during the summer months, they can still have an impact on local rainfall (De Kock et al., 2021). Maphugwi (2026) implemented a shape complexity index (SCI; Lindsay 2018) feature that attempts to only retain storms which contain a structural integrity (i.e. compactness, cohesive cloud shields) for the majority of their lifetimes. By implementing the SCI filter, many fronts were removed from the MCS database.

iv. *Removal of southwest Indian Ocean tropical cyclones:* Over the southwest Indian Ocean, TCs commonly occur during the months of late November through to April with around 10 per season (Mavume et al., 2009; Malan et al., 2013). Although very few of these systems make landfall (Reason and Keibel, 2004), they can make a meaningful contribution to the region's rainfall (Mawren et al., 2023). To eliminate TCs in the MCS tracking database, tracked systems are compared to the TCs found in the International Best Track Archive for Climate Stewardship (IBTrACS) TC v4 database (Knapp et al., 2010; Gahtan et al., 2024). Any MCS that occurred within a 500 km radius of a TC centre within a ± 3-h temporal window of the TC's reported position in IBTrACS is filtered out of the database.

In summary, the results of this study are based on the MCS climatology produced by the modified PyFLEXTRKR run performed by Maphugwi (2026), with the workflow shown in Fig. 2. MCSs are identified and tracked based on the following criteria:

1. Cold cloud systems with a T_b threshold of 235 K (−38.15 °C), a cold core with $T_b < 221$ K (−52.15 °C) and a minimum area (area > 40,000 km^2)
2. The cold cloud system selected in (1) must contain at least five pixels with a precipitation rate greater than 2 $mm.hr^{-1}$, no heavy rainfall component and precipitation feature (PF) major axis with length > 100 km.
3. PF area, mean rain rate, rate skewness and heavy rain volume ratio larger than corresponding lifetime dependent thresholds and,
4. Criteria (1), (2) and (3) must occur continuously for 4 h or more.
5. Systems within ~500 km of a TC are removed from the database
6. A two-tier SCI framework, where the SCI is first applied to the contour representing the 40th percentile threshold of T_b of the identified feature and then on a set 225 K (−48.15 °C) value. A feature that has an SCI > 0.5 for 50% of lifetime is filtered out.

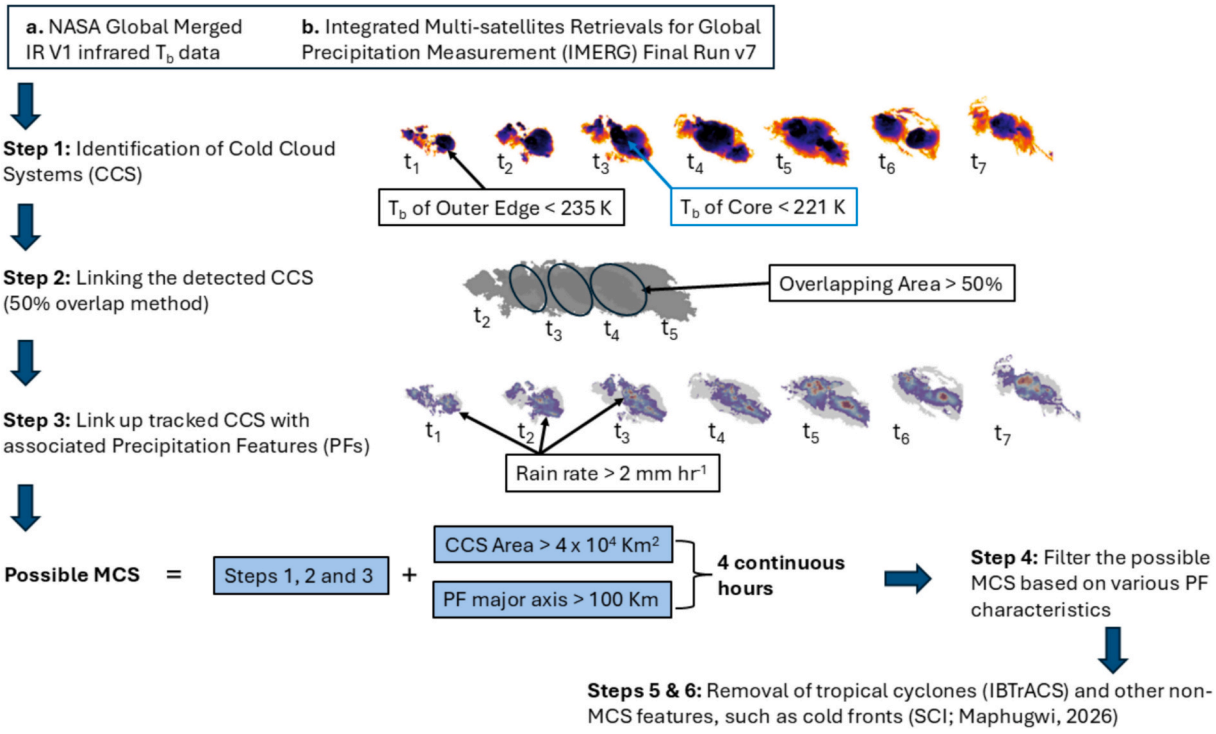

Fig. 2. This schematic summarises the methodology used to develop the regionally tuned MCS database. The two main differences between the methods here compared to the original work of Feng et al. (2021) is that (i) no "heavy rainfall (>10 mm hr^{-1})" threshold is included in Step 4 and that (ii) the SCI methodology developed by Maphugwi (2026) is applied to remove non-MCS cold cloud features.

However, for comparison purposes with other MCS contribution studies, the results obtained using the original settings of PyFLEXTRKR (cold cloud temperature threshold of 241 K / -32 °C, both the −2 mm. hr^{-1} and 10 mm.hr^{-1} rainfall thresholds are used and no SCI filter included), as well as a T_b only run (cold cloud threshold of 235 K / -38.15 °C and no rainfall requirements) are included in the *Discussion* and *Supplementary Material*. Similar to the T_b only run, another run is performed where all deep convective systems (DCSs), regardless of size or duration and with no precipitation criteria included, are tracked. Here, all cloud systems with a Tb < 235 K (−38.15 °C) are tracked and are used to better understand general convective activity during the summer across southern Africa.

The input data used to build the southern Africa MCS database with PyFLEXTRKR includes both the NASA Global Merged IR V1 infrared T_b data (Janowiak et al., 2017) and the Integrated Multi-satellites Retrievals for Global Precipitation Measurement (IMERG) Final Run, version 7 (Huffman et al., 2020). The T_b data is generated by merging observations from various geostationary satellites and provides IR T_b at a spatial resolution of 0.04° and a temporal resolution of 30 min over 60°S to 60°N from 1 January 2000 to present. For consistency in the tracking program, the T_b data was conservatively regridded to a 0.1° × 0.1° resolution using the Earth System Modelling Framework (ESMF; Collins et al., 2005) and resampled to hourly intervals to match the resolution of the precipitation dataset (see *Section 2.2*).

2.2. Rainfall and lightning detection network data

NASA/Goddard Space Flight Center satellite product IMERG version 7 (same as above), hereafter IMERG (Huffman et al., 2020, Huffman et al., 2023) is used as the rainfall product for the analysis. IMERG has a native spatial resolution of 0.1° (~10 km), with rainfall estimates produced every 30 min. IMERG covers the period 2000 onward, but for consistency with the lightning data (discussed below), only data for the period 2010–2024 is used for most of the analysis. It is only in *Section 3.4* where the full 2000–2024 MCS database is used.

Compared to other rainfall products, such as ERA5 (Hersbach et al., 2020) or CHIRPS (Funk et al., 2015), the IMERG product remains relatively untested over southern Africa. However, Thoithi et al. (2023) show that in the extreme rainfall event in April 2022 off the east coast of South Africa, the IMERG product produced consistent rainfall totals (and spatial pattern) with those observed by rain gauges, whereas many other products severely underestimated the rainfall. Similarly, the results of Van Schalkwyk et al. (2025), documenting a MCS in central South Africa, suggest that IMERG produced a reasonable representation of rainfall totals and distribution for the event when compared to weather stations. Furthermore, IMERG remains a commonly used dataset in global MCS rainfall studies (e.g. Feng et al., 2021, 2023b). The IMERG product is also an updated version of the now discontinued TRMM/3B42 satellite dataset (Kawanishi et al., 2000), which was previously used for MCS rainfall analysis in South Africa (Blamey and Reason, 2013). For more discussion on some of the strengths and limitations of IMERG, see Huffman and Tan (2023).

Hourly cloud-to-ground lightning stroke data were obtained from the South African Weather Service (SAWS) for the period 2010 to 2024 and gridded to match the resolution of IMERG data at 0.1° horizontal resolution. The lightning dataset is produced by the South African Lightning Detection Network (SALDN), which comprises 24 Vaisala lightning sensors across South Africa and 1 sensor in neighbouring eSwatini (see Fig. 1b for sensor locations). The network of sensors making up SALDN work together to detect and locate each lightning stroke across the region (Gijben, 2012). The advantage being that even if one sensor is offline for technical reasons, several other sensors within the network will still be able to detect the lightning strokes. As such, the SALDN has an estimated flash detection efficiency of greater than 90% and a stroke location accuracy of less than 0.5 km over South Africa for cloud-to-ground lightning based on a model that statistically self-evaluates the performance of the network on a continuous basis (see Fig. 1 of Gijben, 2012). However, the detection efficiency decreases farther away from the border of South Africa where it drops below 70% at approximately ~4° beyond the border. Recent evaluations of the SALDN against

ground-truth high-speed camera footage of lightning in Johannesburg (South Africa) have found flash detection efficiency of 84.9% (206 high-speed camera events) and median location accuracy of 59.2 m (98 high-speed camera events) (Fensham et al., 2023).

For the purpose of this study, even though the SALDN system is capable of detecting the portion of intracloud lightning, only cloud-to-ground lightning is used here. This is because cloud-to-ground lightning observations are ideal for studies where the impact of lightning is a concern (Simpson, 2013; Gijben and De Coning, 2017; Essa et al., 2022). As described earlier, this is particularly the case for South Africa where lightning-related deaths in the country are considerably higher than the global average. It is not only the local population that lightning presents a major hazard too, but also the aviation industry, sporting events, power companies, forestry managers and firefighting teams (Price, 2013).

2.3. Calculating MCS contributions: The December 2020 MCS example

The process used to isolate the fraction of rainfall and lightning attributed to the MCSs is highlighted in Figs. 3 and 4. During the late afternoon/evening of 23 December 2020, a series of convective storms initiated along the east coast of South Africa, bordering eSwatini and southern Mozambique. These storms intensified and merged under one cloud shield, reaching MCS status during the night, before decaying in the early hours of 24 December 2020 (Fig. 3a). As documented previously, the typical life cycle of MCSs in eastern South Africa is of a nocturnal nature. With storms triggering along the escarpment in the early afternoon, tracking eastwards towards the Agulhas Current in the evening and lasting through to the early morning hours (Blamey and Reason, 2012; Morake et al., 2021). What makes the 23 December 2020 event of interest was the impact it had on local communities, with three fatalities due to lightning in northern KwaZulu-Natal (TimesLIVE, 2020) and considerable damage to infrastructure, destroying homes across the eastern parts of South Africa.

From the cloud shield that delineated the MCS at the given time, a polygon was created (Fig. 3b). This was done for each timestep of the full life cycle of the MCS. Then at each given time step, the IMERG rainfall and SALDN lightning data were extracted that fell within the polygon (Figs. 3c-e). Note that short-lived non-MCS tracks that merge with or split from the identified MCSs are also retained during the tracking. As such, the cloud mask associated with these merge/split tracks are included as part of the MCS cloud shield. The extracted data were then combined to determine the total rainfall, lightning stroke count and spatial coverage of each MCS (e.g. Fig. 4a-b). From these totals, the fraction of rainfall / lightning of each system (or systems) could then be calculated. As a brief example, Fig. 4 c-d provides the fraction of December 2020 rainfall and lightning attributed to the MCS of 23–24 December 2020. Here, it is evident that up to 70% of the December 2020 rainfall was linked to this one MCS, while up to 90% of the December 2020 lightning ground stroke count is linked to the system. The largest contribution to both total rainfall and stroke count over land occurred in the region where the system was positioned during the early phases of the MCSs life cycle. The considerable impact of MCSs on individual monthly rainfall totals in South Africa has been documented before in limited case studies (e.g. Blamey and Reason, 2009; Van Schalkwyk et al., 2025).

The sum of all the MCS rainfall and lightning stroke count were then taken for each austral summer period (October–March; ONDJFM) between 2010 and 2024. By doing so, the fraction of rainfall and lightning linked to MCSs over southern Africa over this 14-year period could be calculated. Note that just for *Section 3.4*, the analysis considers the full MCS database, which covers the period 2000–2024.

3. Results

3.1. Convective storm frequency

This link between convective activity and rainfall in eastern South Africa is highlighted in Fig. 5. Here, any cold cloud systems with a T_b less than −38 °C are tracked through time (i.e. no spatial or duration criteria are applied to these cloud features whereas MCSs such criteria would also be imposed). The heaviest mean rain rates ($\geq$ 4 mm.d^{-1}) during the summer (Fig. 5a) occur around the eastern escarpment, eastwards towards the Agulhas Current. Similarly, this eastern region of South Africa receives the highest frequency in lightning days ($\geq$ 30 days per summer; Fig. 5b) and general convective storm activity ($\geq$ 80 storms per grid cell per summer; Fig. 5c). This part of southern Africa is considered more susceptible to summer convective storms and associated floods than elsewhere in the region due to the nearby presence of the warm Agulhas Current and significant gradients in topography. Garstang et al. (1987) described how the interaction between the topography of the north-eastern escarpment in South Africa and the upper air westerly waves propagating across the southern tip of Africa can lead to the development of strong convection over the east coast of South Africa. The higher storm count than lightning days is due to the way the storm count is determined. Here, each cold cloud system is tracked through time, and a single polygon is then created from this sequence of individual time-steps, irrespective of the time or day. These polygons are then added up for each summer to create a cold cloud shield frequency per grid point. On the other hand, the lightning day frequency is determined on a daily time scale and with a minimum threshold of 10 strokes per day in place.

As with general convective storms shown in Fig. 5, MCSs are most frequent along the eastern parts of South Africa, eSwatini and southern Mozambique (Fig. 6). As found in earlier studies (Blamey and Reason, 2012; Morake et al., 2021), the majority of these MCSs originate over land and track eastwards towards the neighbouring ocean (Fig. 6a). Maxima in both MCS frequency (count and hours) are at a peak over northern KwaZulu-Natal and Mpumalanga provinces in South Africa and eSwatini (Figs. 6b-c). The difference between MCS count (described above) versus hours is that the latter is the count of every hour where a MCS cloud shield occurs over a given grid point. On average, a maximum of 25 MCSs per grid cell and over 100 h of MCS activity are found across South Africa and eSwatini during the summer. The location in maximum MCS frequency is also evident in the rain rates (Fig. 5a) and lightning activity (Fig. 5b). However, the maximum in convective activity of all cold cloud systems is found further south, along the eastern escarpment (Drakensberg Mountain Range) closer to Lesotho, bordering southern KwaZulu-Natal (Fig. 5a), than for MCSs which are nearer eSwatini and northern KwaZulu-Natal (Fig. 6b).

When breaking down either general convective or MCS activity to a monthly time frame, it is evident that there is a distinct seasonal cycle present. Although MCSs are found to occur throughout the summer, Fig. 7 shows that mean MCS frequency is at its lowest during the transitional months of October and March. The equivalent figure showing general convective activity (deep cold cloud systems with no temporal or spatial requirements) at the monthly timescale is found in the *Supplementary Material* (Fig. S1). Frequent MCS activity starts in November (Fig. 7b) over eastern South Africa, eSwatini and southern Mozambique and then peaks during December (Fig. 7c). This is followed by a sharp decline in MCS activity starting in January (Fig. 7d). Spatially, there is a gradual southward (poleward) shift in MCS activity during the summer. During the early summer months, MCS activity is centred across eastern South Africa (northern KwaZulu-Natal and Mpumalanga Provinces), eSwatini and southern Mozambique. During the late summer months, MCSs activity is mostly restricted to the east coast of South Africa, centred over the Eastern Cape and KwaZulu-Natal Provinces. This MCS seasonal cycle, where MCSs are most frequent during November–January, with a peak in December, has been documented in earlier studies using different datasets / methods (e.g. Blamey and Reason, 2012).

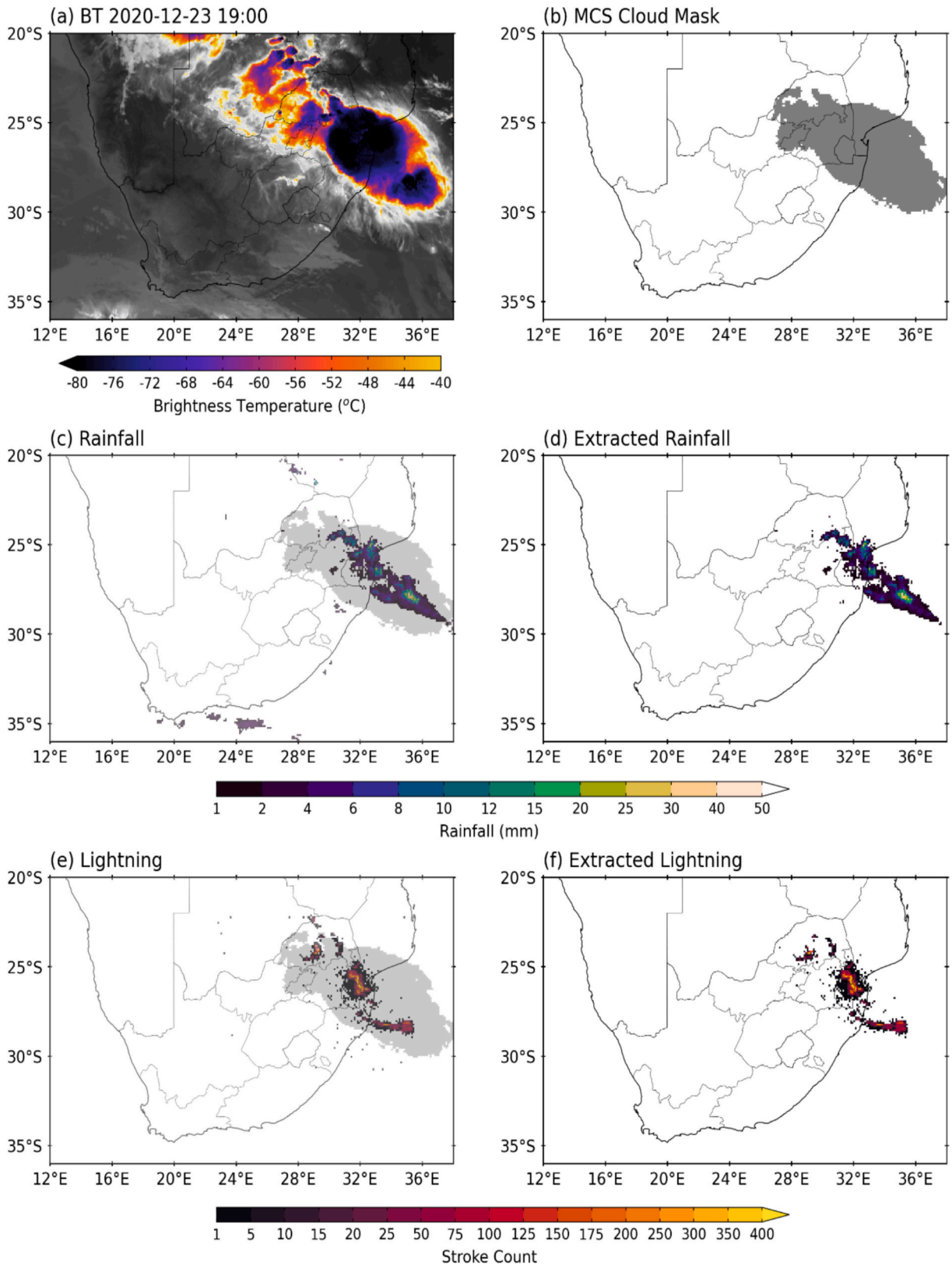

Fig. 3. (a) An example of the cold cloud top (shaded, °C) of a MCS over the southeast coast of South Africa at 19 h00 UTC (LST = UTC + 2 h) on 23 December 2020, (b) the cloud shield polygon (grey colour) at the given time step, (c) the rainfall (mm) estimated by IMERG data for that hour (19:00–20:00), (d) the rainfall extracted based on the MCS polygon in panel (b). Panels d and e, are the same as the rainfall, but for SALDN lightning stroke count.

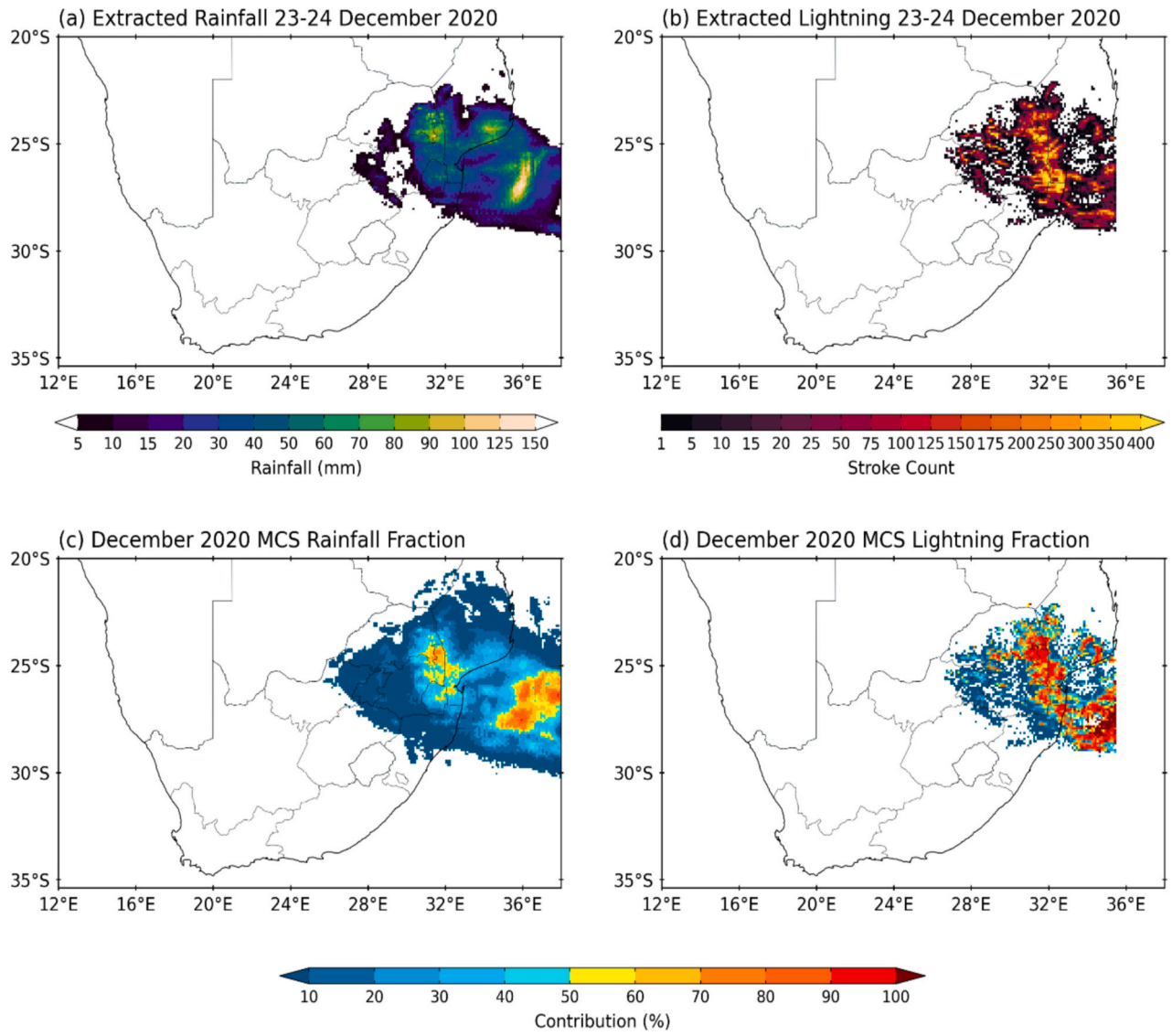

Fig. 4. (a) The total rainfall linked to the MCS event on 23–24 December 2020, (b) the lightning associated with the same MCS, (c) the fraction (%) of December 2020 rainfall attributed to the MCS and (d) the fraction of December 2020 lightning strokes attributed to the MCS.

Morake et al. (2021) suggested that this seasonal cycle in MCS activity could be attributed to the more favourable CAPE and vertical shear profiles for sustained convection to occur across eastern South Africa during November–December.

3.2. *Summer MCS rainfall and lightning contributions*

Summer rainfall linked to MCSs is mostly restricted to the eastern half of subtropical southern Africa (Fig. 8a). Although most of the eastern region receives rainfall from MCSs, the highest rain rates are located in northern KwaZulu-Natal, Mpumalanga, southern and central Mozambique (Fig. 8a). As such, it is found that MCSs make a reasonable contribution (≥25%) to the summer rainfall across most of eastern South Africa, Mozambique, Zimbabwe and east Botswana (Fig. 8b). Fig. S2 shows the Coefficient of Variation (CV) of the contribution of MCSs to summer rainfall across the region. The CV is a metric used to evaluate the variability from the mean (Lovie, 2005), with applications typically to rainfall data (e.g. Asfaw et al., 2018). The relatively low to moderate CV values (<30) indicate that there is generally some consistency in the contribution made by MCSs to the summer rainfall for these regions in eastern southern Africa.

The maximum mean summer contribution occurs in central Mozambique (≥45%), with the rest of southern Mozambique, north-eastern South Africa and southeast Zimbabwe recording a mean contribution in excess of 35%. This region of southern Africa is also impacted by occasional landfalling tropical cyclones (Mawren et al., 2023) which, on average, contribute 10–20% to rainfall totals but this average is biased by a few very strong events such as TC Eline in February 2000 (Reason and Keibel, 2004) or TC Idai in March 2019. Since tropical storms and cyclones also have a cold cloud top, large size and long duration, they could easily be mistakenly tracked in automated MCS methodologies (Feng et al., 2019). However, as noted in *Section 2*, all tropical storms or cyclones tracked in IBTrACS are removed from the MCS dataset used here.

Although central South Africa (Northern Cape, western and southern Free State, North West Provinces) is part of the summer rainfall region, MCSs do not have as great an impact there as that found in the east of the country, with a mean contribution ranging from 10 to 25% (Fig. 8b). There is, however, considerable variability in the MCS summer rainfall contribution across this region, with CV values exceeding well over 40 for most parts (i.e. high variability; Fig. S2). This section of the country is considerably drier than the rest of the summer rainfall region with less

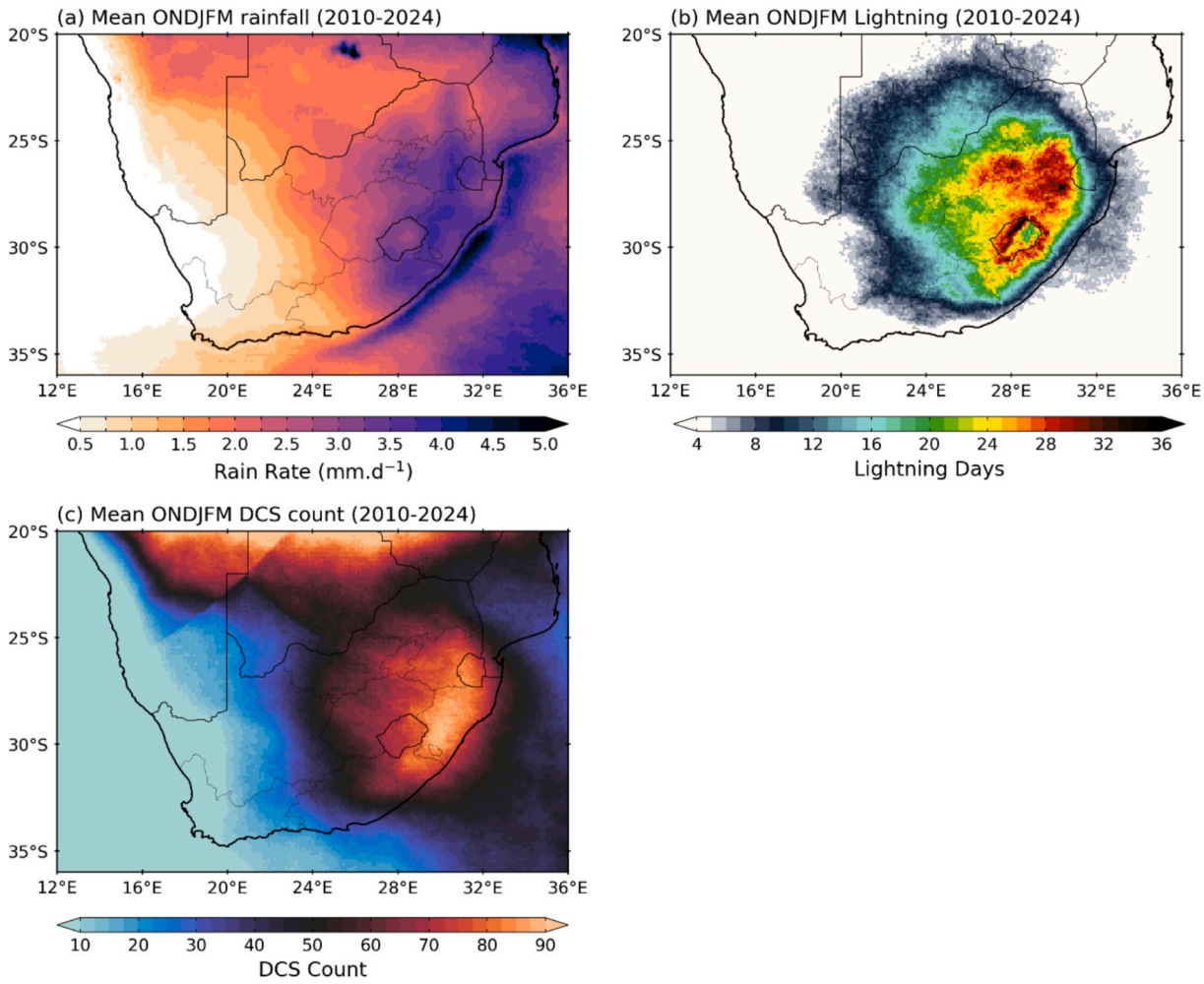

Fig. 5. (a) Mean ONDJFM rain rate based on IMERG rainfall data (shaded; mm.day-1), (b) mean ONDJFM lightning days from data produced by the SALDN and (c) mean ONDJFM deep cold cloud systems (DCS) tracked in PyFLEXTRKR. A DCS in panel (b) is considered as any cloud system, regardless of size and shape, tracked in PyFLEXTRKR with a cloud top temperature (Tb) less than −38.15 °C (235 K). It is used here as a proxy for convective storm development over southern Africa. A lightning day, used in panel (b), is defined as a day when 10 or more strokes occur within the grid on a given day. All panels are averaged over the 2010–2024 period.

frequent MCSs on average (Figs. 5a and 6b, respectively). However, when MCSs do occur here, they can make a considerable impact, such as the summers of 2018/2019 and 2023/2024, with contributions well over 50% produced by a single system (e.g. Van Schalkwyk et al., 2025). The same applies for the dry regions to the north in Namibia and southwestern Botswana.

During the summer, MCSs make a considerable contribution to lightning activity over eastern South Africa, eSwatini, southeast Zimbabwe and Mozambique (Fig. 8c-d). In fact, more than half the lightning activity can be traced back to MCSs over these regions. For the rest of South Africa, most provinces in the central or eastern half of the country have at least 20% of the summer lightning activity linked with MCSs. As shown earlier, the lightning distribution around South Africa is mainly centred around the eastern escarpment, from southern Lesotho, northwards along the KwaZulu-Natal to Mpumalanga provinces. A secondary hotspot is evident inland, over the Highveld, containing Gauteng Province, the key economic and industrial hub in South Africa (Fig. 5b). This result highlights that apart from the eastern parts of South Africa, into eSwatini and Mozambique, other forms of convective storms potentially play a bigger role in lightning production when compared to MCSs.

As with rainfall, when MCSs occur in regions with infrequent convective activity, such as over the drier inland region of central South Africa, into southern Namibia and Botswana, they can be responsible for producing nearly all the lightning (≥80%) for the region for that season (*not shown*). The same applies to the neighbouring ocean, off the east coast of South Africa and Mozambique, where lightning activity is not as frequent compared to that over land (Fig. 5b). Here, MCSs on average contribute to well over 50% of the mean summer lightning activity (Fig. 8d), but it can be over 80% in some summers (*not shown*). Considering differences between MCS rainfall and lightning contributions, we find most regions where MCS rainfall contribution is relatively reduced compared to lightning to be associated with warmer mean MCS brightness temperatures (Fig. S3), particularly towards coastal regions and over the ocean. This is in line with a gradual transition to more maritime convective types, suggesting that warmer, less electrified rainfall-producing systems contribute strongly to rainfall totals in these regions, reducing MCS rainfall contribution versus lightning.

Although a full storm-environment composite analysis is beyond the scope of this study, the observed spatial patterns in MCS rainfall and lightning contributions are broadly consistent with the climatological distribution of environmental conditions favourable for organised convection over eastern southern Africa (Fig. S4). In particular, southern Mozambique and northeastern South Africa coincide with relatively large CAPE, enhanced low-level humidity and stronger deep-layer shear along and east of the steep escarpment. This likely supports both the high MCS frequency and the large lightning contribution in this region (cf. Fig. 8a,c). By contrast, MCS maximum rainfall contribution occurs

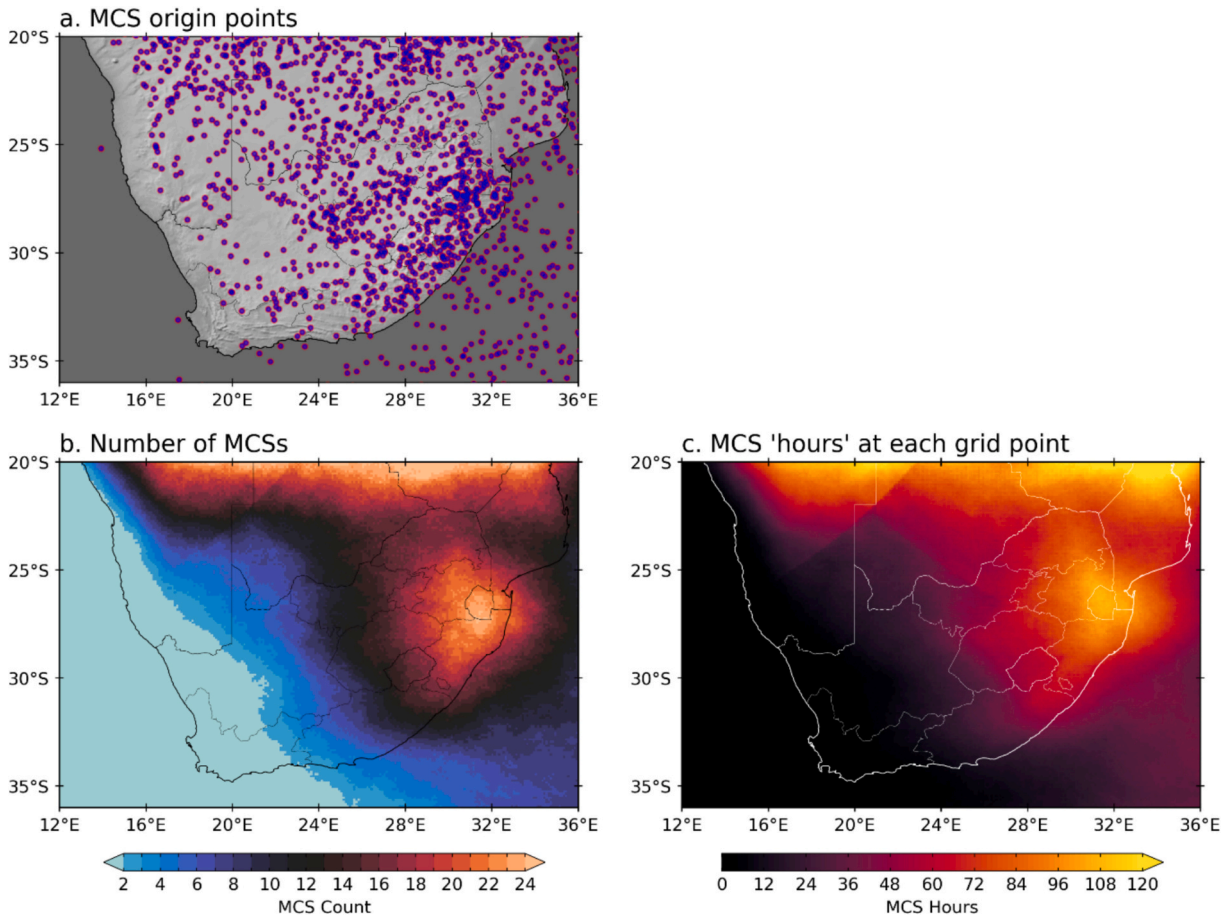

Fig. 6. (a) The origin points of MCSs during the austral summer months (ONDJFM) across southern Africa over the period 2010–2024. (b) The mean number of MCSs per grid point during the summer months. The mean number of MCSs per each grid point was calculated by creating a polygon from the cloud shield of each MCS across its entire life cycle and then summing each polygon together and divided by the number of seasons. (c) The mean number of hours for which MCSs occur at each grid point during the summer months. Calculated by summing up the cloud shields of each MCS (hourly intervals) and dividing by the number of seasons.

farther north over the more humid low-lying coastal plain, suggesting that moisture availability and longer MCS residence times in this area may be especially important for accumulated rainfall, whereas instability appears more closely tied to lightning production, as found in previous studies (e.g. Bang and Zipser, 2016).

3.3. Seasonal breakdown in MCS rainfall and lightning contributions

One of the challenges with climatological studies is in choosing an appropriate season to analyse the data. Excepting the small winter rainfall region, typically averaging weather patterns over southern Africa for a full austral summer (Oct-Mar), the core summer months (Dec-Feb) or sometimes breaking the summer half of the year into bi-months is done. Fig. 7 highlighted that there is a strong intra-seasonal pattern in MCSs frequencies across southern Africa while Fig. 9 shows that the same is true in MCS monthly rainfall contributions. The peak months where MCSs make the largest contribution to seasonal rainfall are November and December. The highest contributions occur in the eastern parts of subtropical southern Africa, with central Mozambique standing out during both November and December (Fig. 9b-c). Here, rainfall contributions from MCSs exceed 50% during December for large parts of Mozambique and for parts of northern KwaZulu-Natal, Mpumalanga and eSwatini. Although MCS contributions during the other summer months are not as great, these systems still contribute over 25% of the summer rainfall for large parts of eastern southern Africa from October through to February. In March, the area where MCSs provide at least 25% of the rainfall is noticeably less than in February but still covers large parts of Mozambique.

For the rest of the region, MCSs have more impact over the interior of South Africa and along the coastal regions, south of northern KwaZulu-Natal, during the late summer months. During the early summer months (Oct-Nov), MCS rainfall contributions in these parts are less than 10% of the monthly rainfall. By January, and continuing in February, the MCS contribution exceeds 20% for most of the Eastern Cape as well as a band to its northwest in the Northern Cape province. This contribution percentage remains evident over the Eastern Cape in March as well as in a small area to its west near 22°E, 32°S.

Similar to the rainfall contributions, large amounts of lightning activity linked to MCSs is restricted mostly to southern Mozambique and immediate surrounds during October (mean contribution over 50% in some places) (Fig. 10a). During November and December (Fig. 10b-c), MCSs make large contributions to lightning from Mozambique west across about a third of South Africa. Unlike that seen in the full summer mean, it is during these two months, but particularly November, when MCSs make a meaningful contribution ($\geq$40%) to the Highveld lightning activity. December is when lightning activity peaks, in terms of MCS contribution, to most of the eastern half of the domain. Here, MCSs account for more than half the entire month's lightning activity in eSwatini and most of Mozambique. As with rainfall, the South African coast, from southern KwaZulu-Natal into the Eastern Cape, appears to have more lightning activity linked to MCS during the late summer months compared to the early summer months (Fig. 10c-e). Even April can show this tendency, (e.g., Fig. S5 and S6), where a single MCS contributed between 80 and 100% (20–60%) in lightning activity

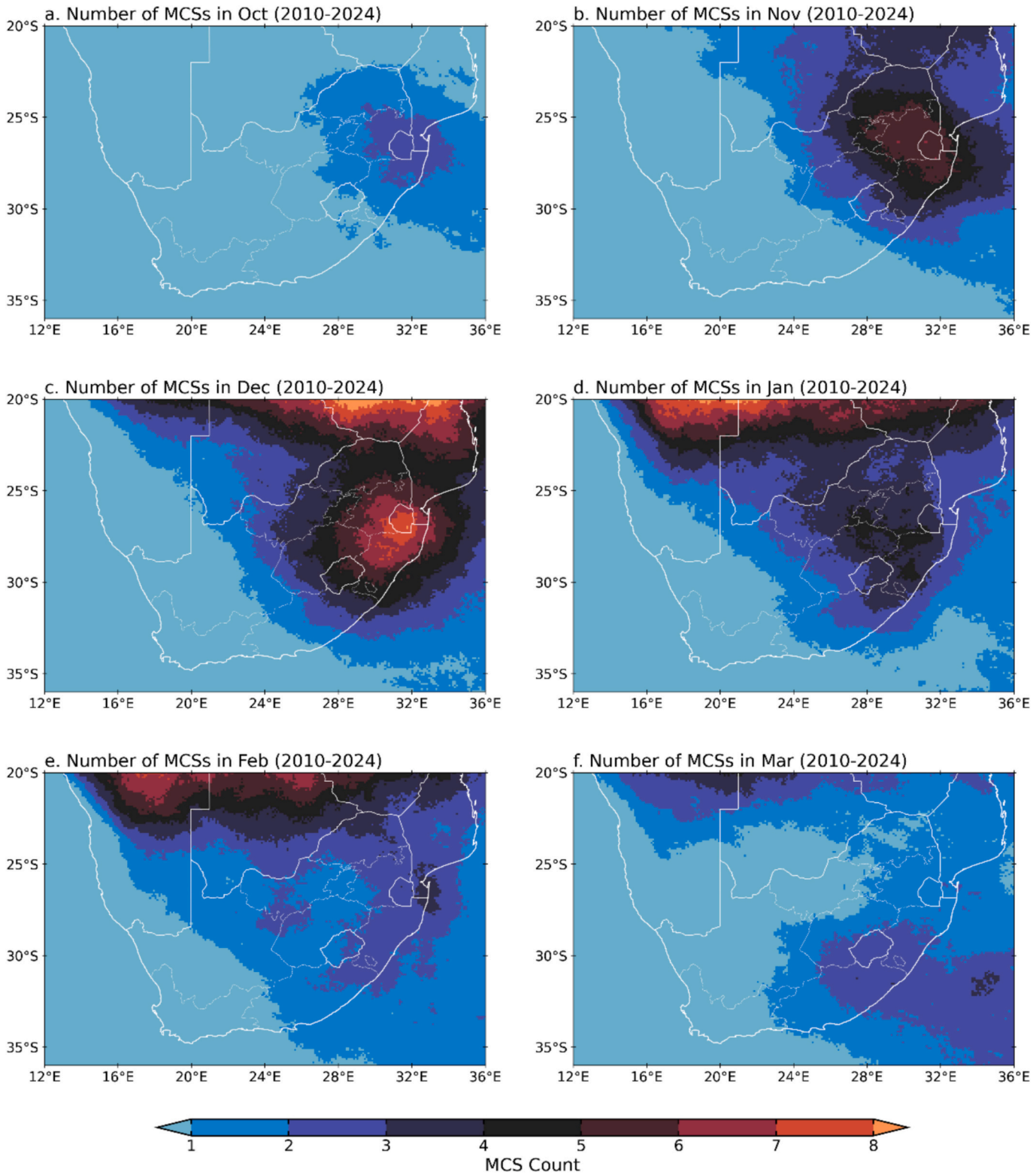

Fig. 7. The mean number of MCSs that occur during the individual austral summer months, from (a) October through to (f) March. This is created by summing up the cloud shield created by each individual MCS timestep to create a single polygon. Then summing up the polygons and dividing by the number of months. It is taken over the period 2010–2024.

(rainfall) along the Eastern Cape and KwaZulu-Natal coastline. On the other hand, MCSs make a considerable contribution to lightning activity for each of the six summer months, in northern KwaZulu-Natal and southern Mozambique.

3.4. Interannual variability and ENSO

The impact that MCSs may have on summer rainfall in the region is more apparent in the contribution to the individual warm season total rainfall (Fig. 11) averaged over the box shown in Fig. 1a. It is evident

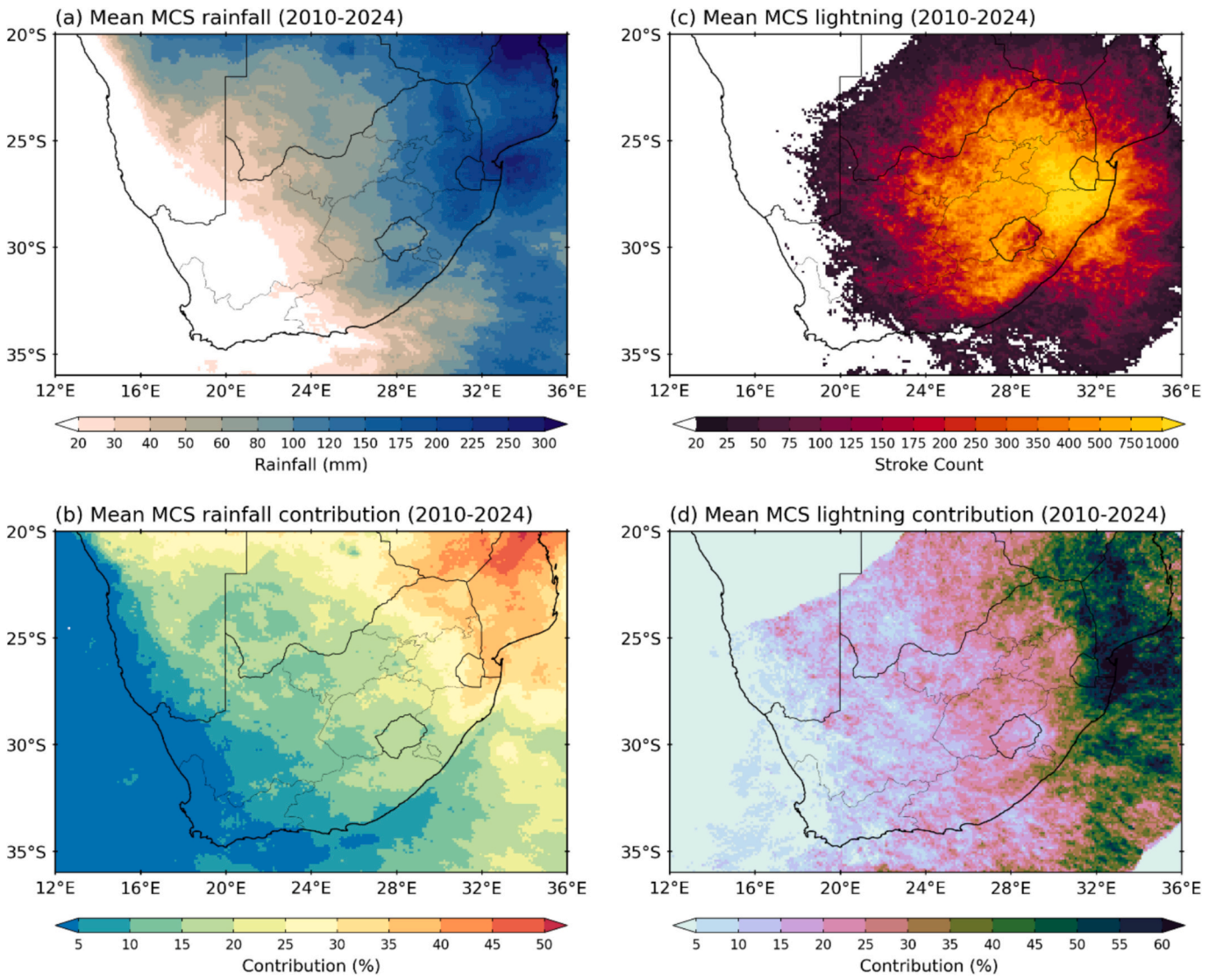

Fig. 8. (a) The mean amount of austral summer rainfall (ONDJFM) produced by MCSs, (b) the mean fraction of rainfall during the summer period attributed to MCSs, (c) the mean amount of lightning strokes produced by MCSs during the summer months and (d) the fraction of lightning stokes attributed to MCSs. This is for the period 2010–2024. Unlike Fig. 5b, which displays lightning spatial frequency based on 'lightning days', the mean lightning count here is determined from individual strokes.

that the region contains considerable interannual rainfall variability (Fig. 11a). Wet years here are considered to have taken place in 2020/21 or 2022/23, with an extremely dry summer in 2015/16. These wet (dry) years correspond to El Niño (La Niña) conditions in the Pacific Ocean, which is consistent for this region (Blamey and Reason, 2023). Although the El Niño-Southern Oscillation (ENSO) is considered the dominant driver behind interannual rainfall variability over southern Africa during summer, there is no conclusive relationship with ENSO and MCS frequencies over eastern South Africa (Blamey and Reason, 2012; Morake et al., 2021). On average, 48 MCS occur within this domain per summer, and it ranges from a minimum of 34 in 2011/2012 to a maximum of 61 systems in 2016/2017 (Fig. 11b). Although some El Niño (La Niña) summers correspond to fewer (more) MCS than average, such as 2014/15 and 2015/2016 (2020/21), this is not always the case. The summer of 2011/12, corresponding to a La Niña summer, had the second fewest MCSs (36) and the summer of 2018/19, an El Niño summer, had an above average number of systems (52). This is consistent with Morake et al. (2021), investigating MCSs in eastern South Africa between 1985 and 2008, also noting no clear relationship between ENSO and MCS frequency. However, the caveat here is that there are few ENSO events to consider using this limited time period and that the time series is developed from a relatively broad area.

Given that the 2010–2024 period has relatively few ENSO events needed to evaluate any meaningful relationship, we extend the rainfall analysis here to cover the full 2000–2024 MCS database. To test the sensitivity of a shortened time period, a correlation between IMERG rainfall and ENSO for the 2000–2024 period is first performed. The correlation between the DJF rainfall and ENSO reveals a consistent ENSO-type pattern for most of southern Africa, where a significant negative correlation exists (*not shown*). This is consistent with the ENSO-southern Africa summer rainfall relationship using alternative rainfall datasets, such as ERA5 (Blamey and Reason, 2023) or CHIRPS (Kekana et al., 2025), over a longer time period. The correlation between the MCS frequency (here, defined as days with an MCS for each summer) also reveals an ENSO-type pattern for most of the summer rainfall region across southern Africa, where a negative correlation exists (*not shown*). To illustrate this, Fig. 12 depicts the core summer (DJF) composites of both standardised rainfall anomalies and MCS days linked to El Niño and La Niña events. As previously documented in the literature, even with only considering ENSO events post 2000, there is typically less (more)

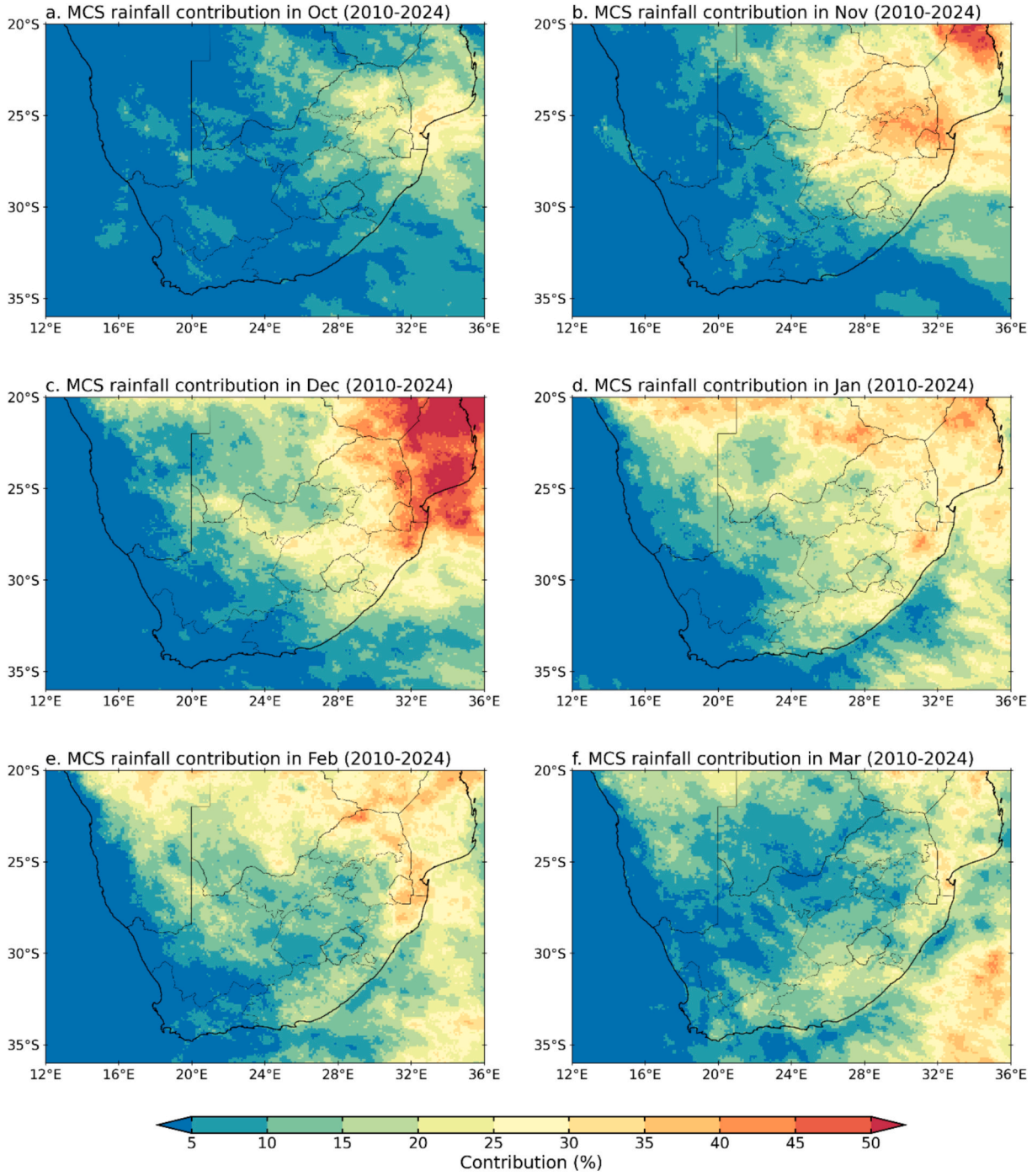

Fig. 9. The mean monthly fraction of rainfall (%) attributed to MCSs from (a) October through to (f) March over the period 2010–2024.

rainfall during El Niño (La Niña) (Fig. 12a and b, respectively). The decrease (increase) in rainfall totals during El Niño (La Niña) are largely linked to changes in the number of rainfall events, particularly those days with moderate rainfall (>10 mm; Fig. S7).

As with summer rainfall, El Niño is linked with fewer MCS days over most of southern Africa, particularly Zimbabwe and central Mozambique (Fig. 12c). Where the El Niño -MCS relationship is a bit more ambiguous is over the eastern parts of South Africa and eSwatini. In fact, a weak positive relationship exists between MCS frequency and ENSO for this domain. Given this relationship between MCS frequency and ENSO, it could help explain why this region in eastern South Africa is generally considered to have a relatively weak negative correlation (not significant) between ENSO and summer rainfall compared to the rest of southern Africa. It also highlights that the ENSO relationship may have been masked in Fig. 11 given the domain used to create the timeseries.

A slightly different relationship exists with La Niña, where the strongest relationship with MCS frequency is centred over the western half of the region, extending from Namibia and Botswana, down into central South Africa (Fig. 12d). Wet summers in this region typically occur during La Niña events (Kekana et al., 2025). The wetter summers during La Niña are largely driven by an increase in moderate rain days (>10 mm) in the region (Fig. S7d). The mechanisms that lead to these wet summers during La Niña are not completely obvious, but Van Schalkwyk et al. (2023, 2024) have highlighted the role synoptic scale drylines play in triggering convection in this region. These authors

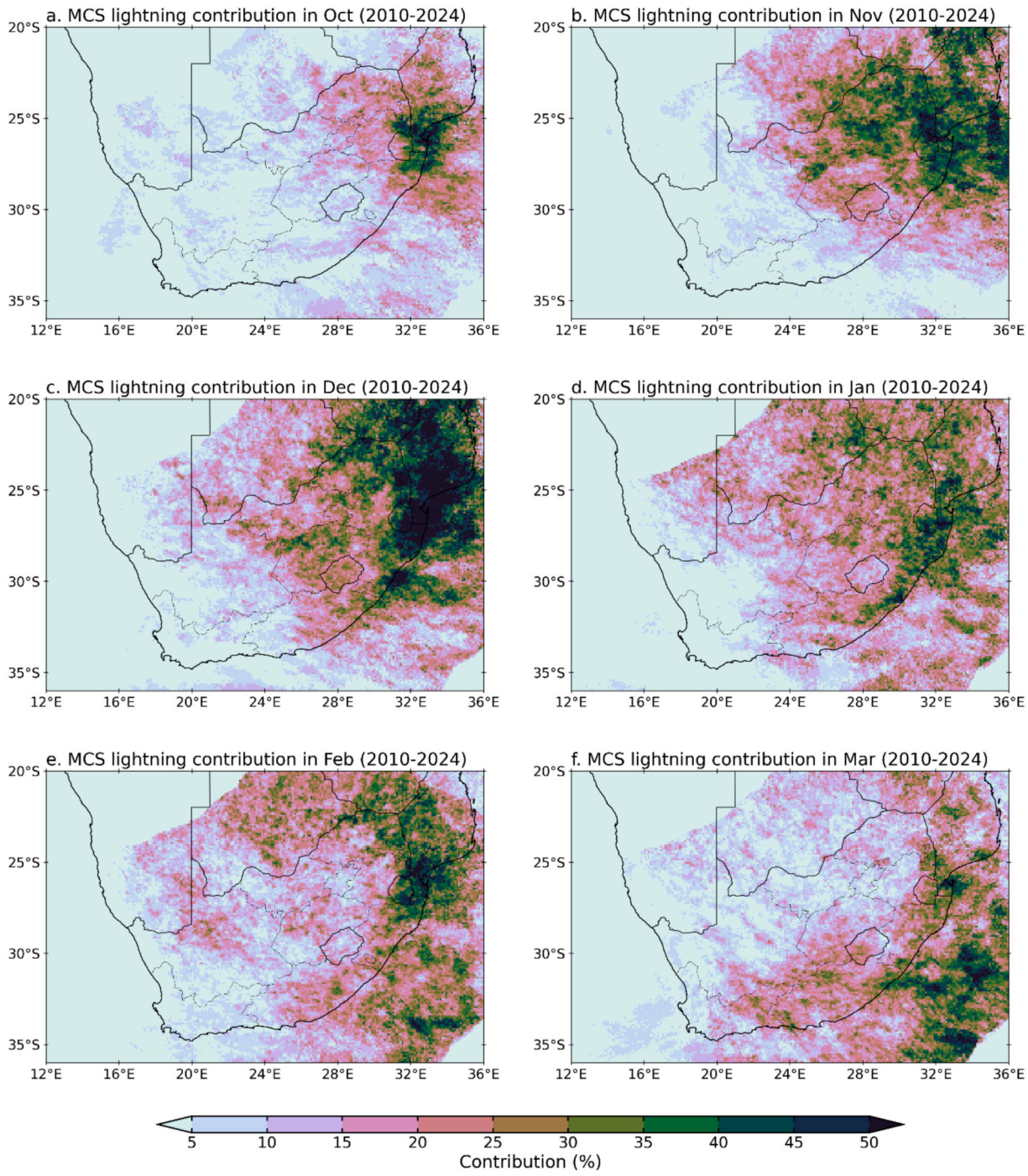

Fig. 10. The mean monthly fraction of lightning strokes (%) attributed to MCSs from (a) October through to (f) March over the period 2010–2024.

suggest that these drylines, which interact with moisture advection from the southwest Indian Ocean, through the Zambezi and Limpopo River Valleys, play a key role in driving convection in this region. Thus, these conditions likely favour MCS development, which is evident in the increase in MCS days during La Niña.

Back to the 14-year period, the mean total summer rainfall contribution by MCSs is 30% over this eastern domain. However, the spread is quite wide when looking at Fig. 8, where MCSs can account for anything from 20 to 50% across this domain. MCSs had the lowest rainfall contribution (~17%) during the 2023/24 summer and the highest contribution (~38%) during 2017/2018 (Fig. 11c). It is interesting to note that there is not necessarily a strong link between MCSs frequency and rainfall totals (and contribution) within this domain. This was also highlighted in the spatial plots where in central southern Mozambique, between 23°S-25°S, MCSs are not as frequent there as that found in southern extremities of Mozambique, into eSwatini and South Africa, or that in northern Mozambique, but still make comparable contribution to summer rainfall across all these regions (see Figs. 6b and 8c).

A direct comparison of MCS frequency and MCS rainfall contribution indicates that the latter is not controlled by system count alone. The spatial distribution for average MCS duration (Fig. 13a) shows that particularly high-contribution rainfall regions towards the north tend to be associated with longer-lived systems that contribute relatively more stratiform rainfall (Fig. S8b,c), with largest MCSs clustering in the northwest and towards the east (Fig. 13b), where stratiform and high intensity convective rainfall act together to increase total MCS rainfall

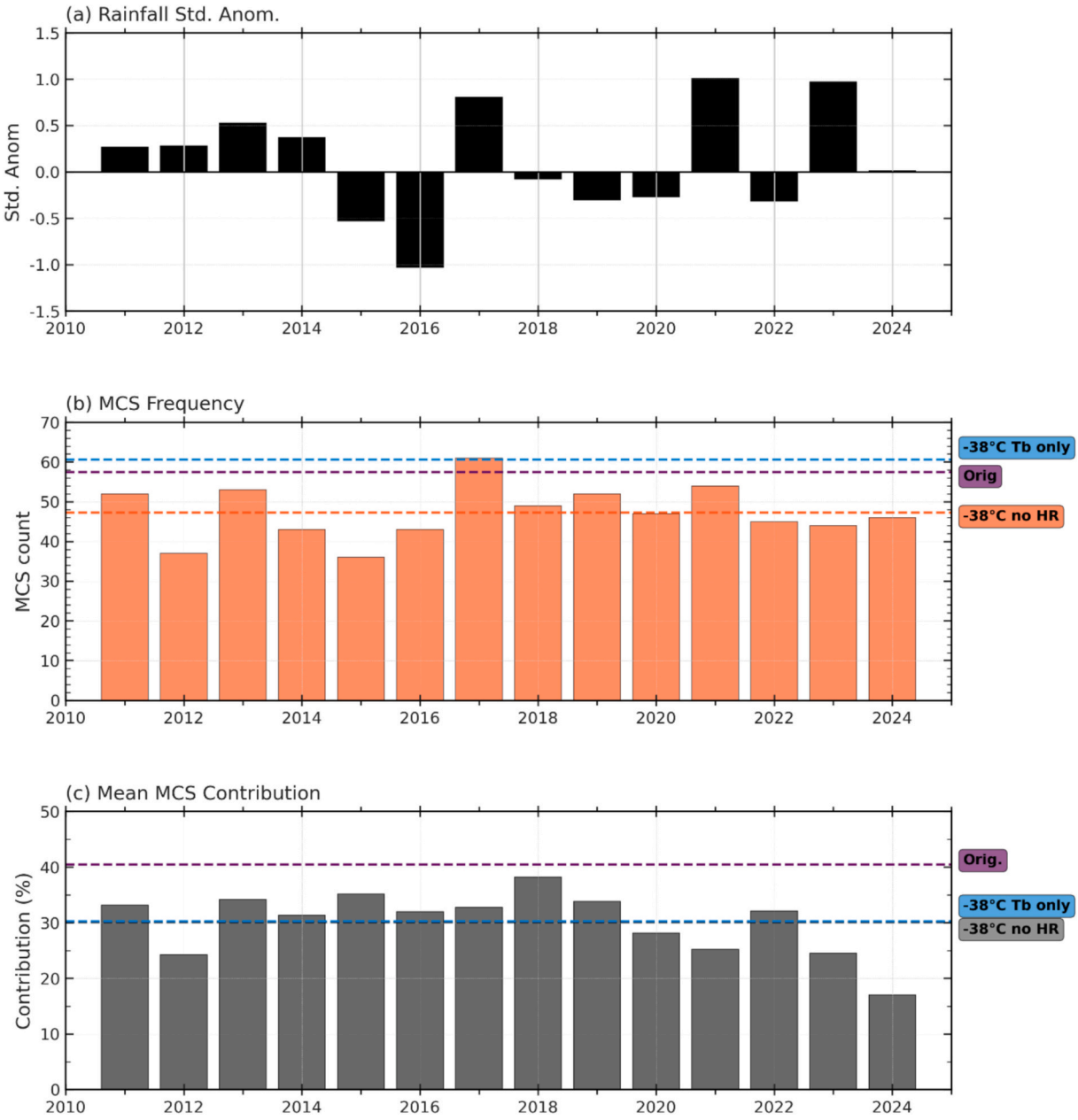

Fig. 11. Bar graphs showing (a) the summer (ONDJFM) rainfall standardised anomalies, (b) the mean MCS count and (c) the fraction of MCS rainfall for the domain shown in Fig. 1a. The first bar is ONDJFM in 2010/11 and the last bar is ONDJFM in 2023/24. Note that the standardised anomalies in panel (a) are based on IMERG data from 2000 to 2024. In panels (b) and (c), the mean MCS count and mean fraction of rainfall attributed to MCSs of the two other sensitivity runs (*Orig*: Purple and *− 38 °C Tb only*: Blue) are also shown. (For interpretation of the references to colour in this figure legend, the reader is referred to the web version of this article.)

disproportionately (Fig. S8d). This behaviour is consistent with Fig. 14 c, d, which shows that MCS total rainfall is linked to both system size and duration. Conversely, high MCS frequency regions with only moderate MCS rainfall contribution, as in some eastern parts of our domain, may arise because the denominator in the contribution calculation includes all rainfall types. Along the eastern escarpment and coastal belt, frequent local convection, orographic rainfall and cloud-band-related precipitation would be expected to increase total rainfall independently of the tracked MCS population, thereby reducing the fractional MCS rainfall contribution even where MCS occurrence is frequent. This result of the rainfall being linked to the size and duration of the system has been documented in other MCS populations (Roca and Fiolleau, 2020). Another possibility of the larger rainfall contribution in central southern Mozambique could be due the clustering MCSs (e.g. Hu et al., 2025). Essentially, the frequency of MCSs in space and time (i.e. clustering) could play a role in some regions in southern Africa receiving more rainfall or having higher rainfall contribution than others that have a similar MCS frequency but spread over the entire season.

4. Discussion

The key results from this analysis highlight the importance of MCSs for both the production of rainfall and lightning over South Africa and neighbouring countries. This was determined using an MCS database that was built from the PyFLEXTRKR automated tracking methodology. The choice for using such an approach, which includes using both T_b and rainfall as part of the MCS detection, is that it aligns more closely with Houze (2004: Pg 1) definition of an MCS - as a "*cumulonimbus cloud system that produces a contiguous precipitation area 100km or more in at least one direction*". Another advantage is that including rainfall

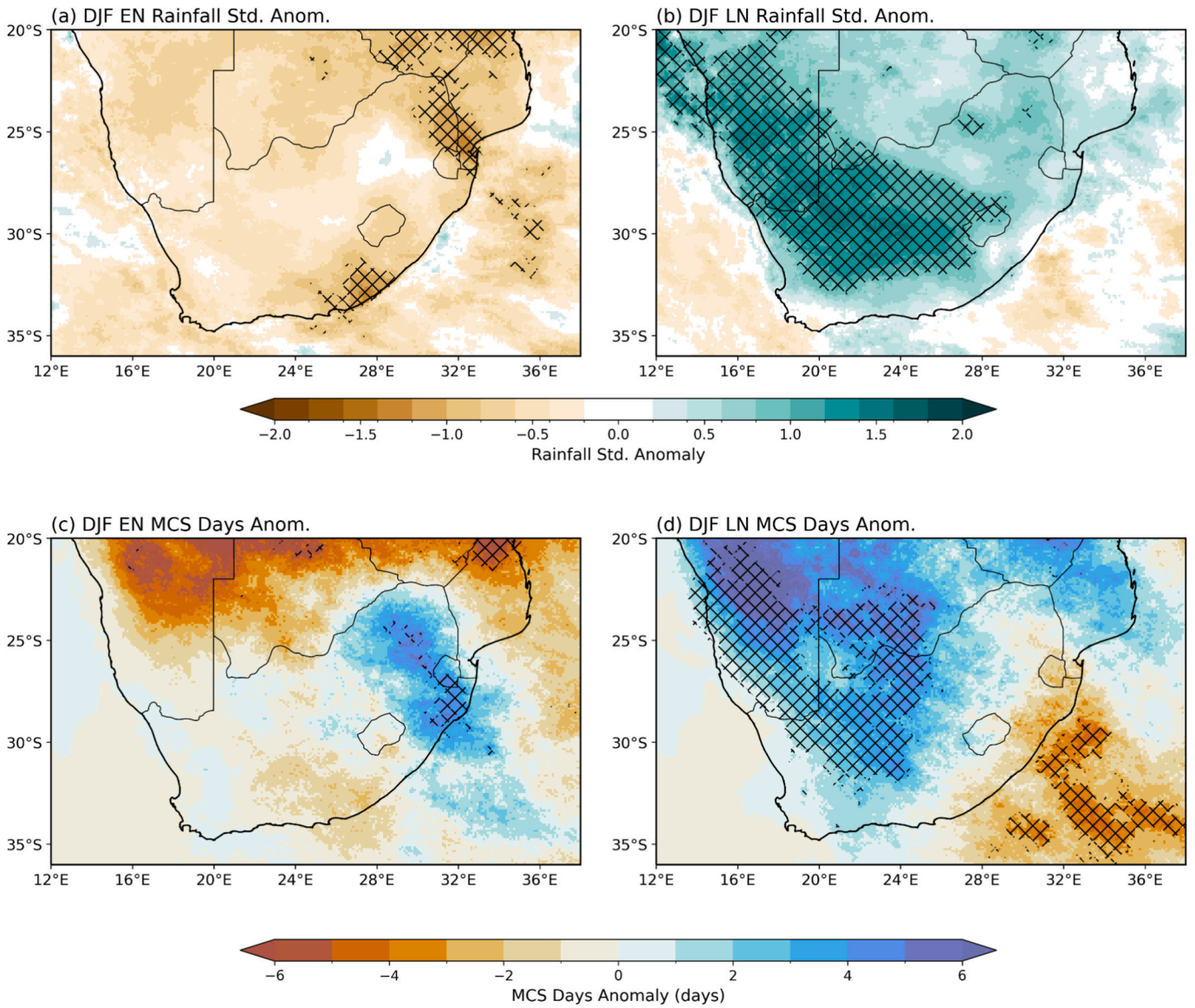

Fig. 12. Composite of DJF standardised rainfall anomalies across southern Africa for the five strongest (a) El Niño years and (b) La Niña years over the period 2000–2024. The ENSO years here are based on the DJF Oceanic Niño Index (ONI) in the Niño 3.4 region, with El Niño years considered as 2002/03, 2009/10, 2015/16, 2018/19, and 2023/24. Similarly, La Niña years are considered as 2005/06, 2007/08, 2010/11, 2020/21 and 2021/22. (c) and (d) are composites of anomalies in MCS days during the five El Niño and La Niña summers, respectively. Hatching in the figure denotes values that are statistically significant at the 95% level based on a two tailed nonparametric Monte Carlo bootstrap significance test.

characteristics as part of the tracking methodology improves detection of MCS, particularly in midlatitude regions (Feng et al., 2021). Along with PyFLEXTRKR, tracking algorithms such as Tracking and Object-based Analysis of clouds (TOBAC; Heikenfeld et al., 2019; Sokolowsky et al., 2023); Forecasting and Tracking the Evolution of Cloud Clusters (ForTraCC; Machado et al., 1998; Vila et al., 2008) and Multi-Object-Oriented Algorithm of Precipitation systems (MOOAP; Prein et al., 2023) consider more than just T_b for the identification and tracking of convective features. However, one key challenge in automated MCS tracking is the lack of standardised identification criteria. Detection criteria such as the T_b threshold often vary from one region to the next. As documented by several studies, such as Feng et al. (2025), rainfall thresholds can also influence MCS identification and tracking across different regions. It is worth highlighting that testing of the different tracking algorithms have been mostly based on tropical environments. Compared to equatorial Africa, where rainfall is more convective in nature, there is generally a higher stratiform rainfall contribution in the subtropical regions (Schumacher and Houze, 2003; Schumacher and Funk, 2023). This suggests that there may be some sensitivity in the results here.

Figs. S9 and S10 show two different MCS frequency maps based on different identification criteria in PyFLEXTRKR (see *Section 2.1* for a complete description). In the original PyFLEXTRKR run, there are considerably more MCSs that are tracking along the eastern parts of South Africa (Fig. S9a-b). There is a clear MCS hotspot to the east of Lesotho, along the KwaZulu-Natal south coast in South Africa. In the earlier analysis, the MCS hotspot was further northwards and inland, centred over eSwatini and the Mpumalanga and northern KwaZulu-Natal provinces of South Africa. The hotspot in the original run extends out from the east of South Africa into the adjacent ocean. As documented in Maphugwi (2026) the greater frequency of MCSs in this region (South West Indian Ocean) is linked to the algorithm identifying more disorganised frontal precipitation features. Another large contrast is that there are also fewer systems that occur along the northern parts of the domain in Botswana, Zimbabwe and Mozambique in the original run. This difference in MCS frequency along the northern parts of the

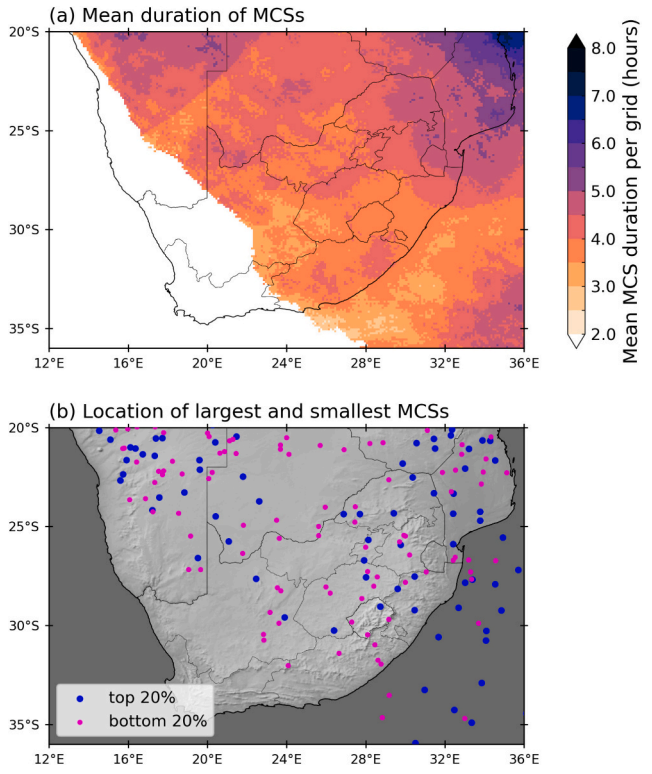

Fig. 13. (a) The mean MCS duration per grid point (hours). The mean MCS duration per grid point is determined by the mean number of hours for which MCSs occur at each grid point divided by the mean MCS count per grid point. Regions that have on average less than 3 MCS per summer are masked out. Panel (b) shows the centre location of the largest (top 20%) MCSs (blue dots) versus the smallest (bottom 20%) MCSs (magenta dots). This was based on the size of the MCSs at the maximum extent during the life cycle. (For interpretation of the references to colour in this figure legend, the reader is referred to the web version of this article.)

domain appears to be attributed to the heavy rain rate requirement in the original run (Maphugwi, 2026). A challenge with the IMERG product is that it may underestimate rainfall intensities over Africa (e.g. Amell et al., 2025), which implies that instantaneous peak rates are missed by the satellite retrievals. This suggests that further work is needed on evaluating the IMERG product in southern Africa to help identify a more appropriate high rainfall rate threshold (if two are used). The removal of the peak rainfall threshold for MCS detection in this study hence aims at reducing the number of missed MCSs due to IMERG rainfall underestimation. Indeed, accurate peak rainfall information may be less crucial than reliable estimates for rainfall totals, given the large raining stratiform anvils and considerable lifetimes of sub-tropical MCSs can cause severe cumulative hydrological impacts.

Alternatively, it is worth considering a different rainfall product as input for PyFLEXTRKR, with the big limitation being the need for hourly data. A common product used in southern Africa climate analysis is ERA5 rainfall (e.g. Mpheshea et al., 2025; Thoithi et al., 2025). However, considering that ERA5 is based on model output, it is susceptible to suffer from the typical "drizzle bias" of models with parametrised convection (Chen et al., 2021). This is where they overestimate low rainfall events and underestimate high rainfall events, which may be problematic for MCS tracking. Another challenge is around how well the rainfall is captured in areas that have frequent convective storm activity, such as that around the topography of southern Africa (Fig. 5). Fig. S11 illustrates the difference in mean DJF rain rate across southern Africa in IMERG, ERA5 and CHIRPS. The largest differences between the products occur along the eastern escarpment of eastern South Africa. IMERG typically has a lower mean rain rate compared to the two other products. Over Mozambique, where MCS make the highest mean contribution, IMERG has a higher mean rain rate than ERA5, but a lower mean rain rate than CHIRPS. It appears that the difference in mean rate is partly related to the mean number of moderate rain days (>10 mm) in each product. This is particularly the case for the CHIRPS product, where IMERG has more general rain days (>1 mm; not shown), but less moderate rain days (Fig. S12) than CHIRPS, leading to the overall lower rainfall total in IMERG. For both ERA5 and CHIRPS, the higher mean rainfall rates compared to IMERG around the eastern escarpment is associated with both these products having more moderate rain days in this region. For the rest of southern Africa, the three products show a lot of similarities in mean rain rates and rain days.

The impact of the different MCS climatology in the original run is evident in the fraction of rainfall and lightning attributed to MCSs (Fig. S13). There is considerably more ONDJFM rainfall and lightning linked to MCSs along the entire eastern coastline of southern Africa, from the Eastern Cape Province in South Africa up into central Mozambique (with a mean exceeding 40% for most of the region; Fig. 11c). There is even a greater contribution over the adjacent ocean area, with mean contribution values exceeding 50%. These values are consistent with the earlier work of Feng et al. (2021) documenting the mean December–February MCS rainfall in the Southern Hemisphere. However, as alluded to earlier, this MCS rainfall contribution in the original settings is perhaps slightly overestimated given that some non-MCS systems are included in the climatology. It is also worth considering the role splitting / merging of an MCSs may play in the original run versus the two other runs using a colder T_b. As documented in Feng et al. (2023a), warmer T_b thresholds in PyFLEXTRKR have a higher fraction of MCSs starting as a split or ending in a merge. It is reminded that here split or merged systems are included in the polygon used to extract the MCS associated rainfall and lightning.

In the T_b-only run (Fig. S10a-b), the frequency maps show many similarities to the climatological run described above. The main MCS hotspots are found over eSwatini and the Mpumalanga and northern KwaZulu-Natal Provinces in South Africa, as well as the countries in the northern parts of the domain. However, based on the mini-domain used to describe MCS interannual variability (see Fig. 3a), it is clear that more MCSs are detected in the T_b-only run compared to that of the original run and the chosen settings run used for the analysis. Surprisingly, this has very little impact on the overall MCS contribution to regional rainfall (Fig. 11c and Fig. S14). Both the chosen run and the T_b-only run have a mean contribution of about 30% to rainfall in eastern southern Africa. There are some minor differences in the lightning contribution though, with the T_b-only run having a slightly higher contribution compared to the chosen run.

Overall, there is a clear sensitivity to calculating the MCS contribution to rainfall and lightning activity in southern Africa based on the criteria used to identify and track MCSs (summarised in Table 1). Here, the mean MCS summer rainfall contributions for eastern southern Africa range from 30%–40% across the three runs. There is also considerable spatial variability in these contribution maps. It is worth noting that this sensitivity is not only linked to MCS identification criteria in PyFLEXTRKR but has also been noted amongst the various MCS tracking algorithms (Feng et al., 2025). Although this does create some challenges for cross regional comparison, the ensemble of tracking algorithms is providing some valuable insight to the importance of such weather phenomena.

5. Conclusion

Convective storms in the central and eastern parts of South Africa have a considerable economic impact through flash flooding, strong winds and destructive hail. The loss of life through lightning activity, particularly in the rural areas, is also a frequent occurrence during the summer months. Globally, it is these types of severe weather events that contribute to the global insurance losses eclipsing over $100 billion for

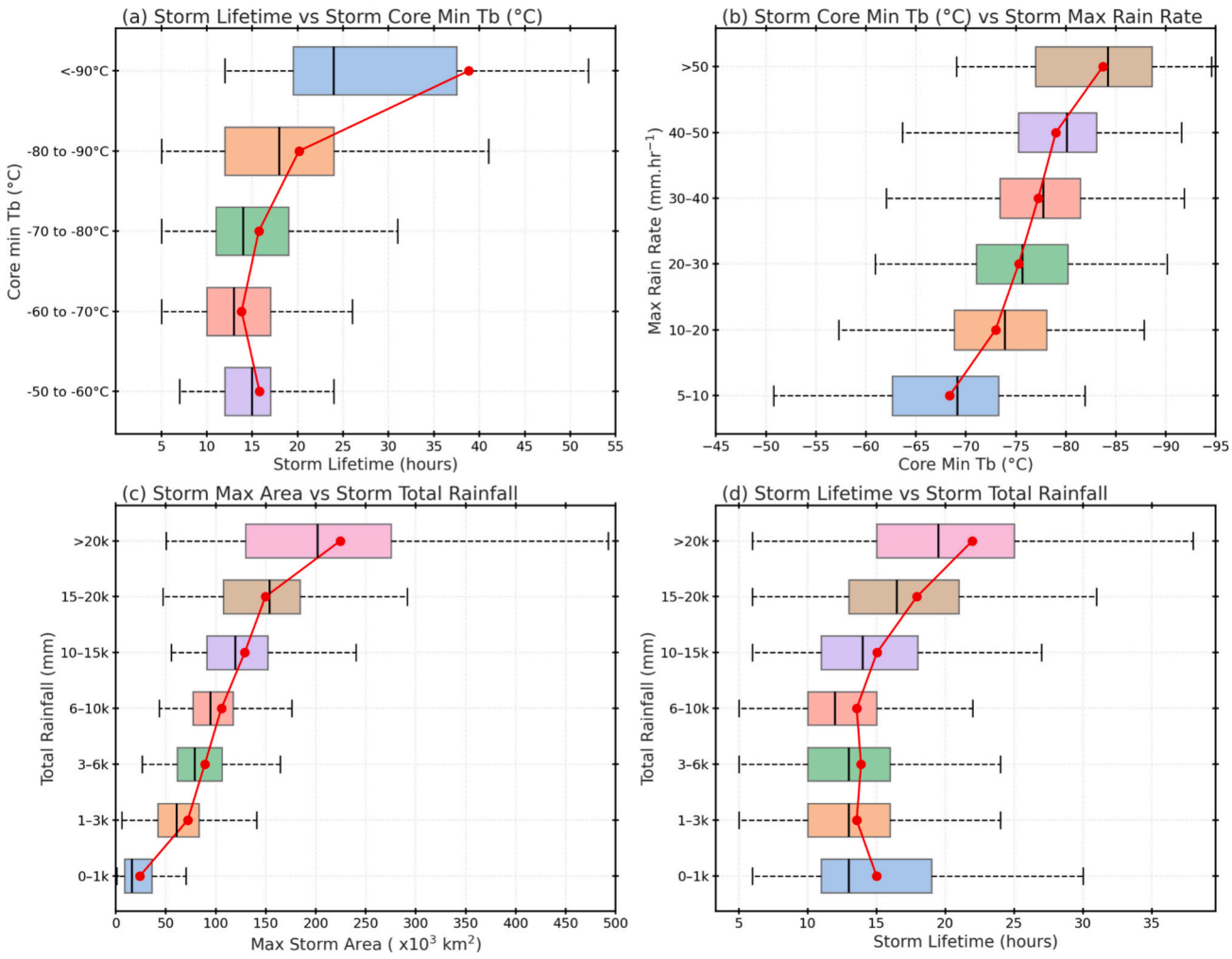

Fig. 14. The whisker plots here depict various characteristics of MCSs found in the eastern southern Africa domain (see box in Fig. 1a) which includes: (a) storm duration (hours) versus the minimum temperature of the cold core (°C), (b) the minimum cold core temperature versus the maximum rain rate, (c) the maximum area obtained versus total rainfall (mm) and (d) storm duration versus the total rainfall (mm). An MCS was included here if at some stage of its life cycle it occurred within the domain. A total of 662 systems were included in the analysis over the 2010–2024 period.

the sixth straight year since 2020 (Gallagher Re, 2025). Thus, understanding the climatological frequency and intensity of such convective extremes in southern Africa is paramount to managing severe weather risk and can help lead to the improvement of catastrophe models, an important tool in the insurance industry, to quantify financial losses from extreme weather events. The focus of this study is placed on the largest of the convective storms, the mesoscale convective system (MCS). Here, the importance of MCSs to southern Africa austral summer rainfall and lightning activity for the 2010–2024 period is quantified.

The MCS database used in this study is produced by Maphugwi (2026) using a modified version of the Python FLEXible object TRacKeR (PyFLEXTRKR; Feng et al., 2023a). Compared to other parts of Africa, MCSs in the southern region of the continent are not as frequent to that in central Africa or West Africa (Feng et al., 2021). However, results in this study show that these systems still make a meaningful contribution (≥35%) to austral summer rainfall, particularly over parts of central and southern Mozambique, southern Zimbabwe, northeastern South Africa and eSwatini. These regions, particularly Mozambique, have previously been documented to experience frequent MCS rainfall (Blamey and Reason, 2013). There is considerable interannual variability with the fraction of rainfall attributed to MCSs over southern Africa. Even over the drier central and west South Africa, MCSs can occasionally produce over half the summer rainfall in a single event (e.g. Van Schalkwyk et al., 2025). Furthermore, more of the rainfall can be attributed to MCSs if one looks at individual months compared to the mean summer season contribution. In particular, the months of November and December are when MCSs make the largest contribution to rainfall (exceeding 50% for the month). However, these regions with high contributions are restricted to northeast South Africa, eSwatini and Mozambique.

Using this new MCS database, a stronger relationship between ENSO and MCS frequency in southern Africa is also found than that documented in earlier studies (e.g. Blamey and Reason, 2009 or Morake et al., 2021). A non-linear relationship exists between ENSO and southern Africa summer rainfall, where typically El Niño events result in less rainfall, while the opposite occurs during La Niña. When using the full MCS database (2000–2024), there appears to be consistency with the ENSO-rainfall relationship in that most parts of southern Africa see a decrease (increase) in MCS frequency during El Niño (La Niña). This is particularly the case for regions such as Zimbabwe and Mozambique where the El Niño-rainfall relationship is often strongest. There is a clear relationship between MCS frequency, rainfall totals and La Niña over the drier western half of southern Africa (Namibia, Botswana and central South Africa). This is likely linked to more favourable conditions that occur in this region, along with regional circulation changes, that favour convection during La Niña (e.g. Van Schalkwyk et al., 2024). The eastern parts of South Africa (including eSwatini) appear to have a more complex ENSO relationship. In contrast to the rest of the summer rainfall

Table 1
The different key criteria used in the three approaches used to identify MCSs in southern Africa is presented in the top half of the table. For easier reading, the bold text in the middle column ('*This study - modified from* Maphugwi, 2026') shows the key parameters used in this study that are different compared to the original PyFLEXTRKR run. The bottom half of the table presents the mean austral summer (ONDJFM) MCS statistics for each of the three runs over the 2010–2024 period for the domain shown in Fig. 1a (eastern southern Africa). The spatial variability of MCS rainfall contribution is illustrated in Fig. S2. The shape complexity index is calculated as: SCI = 1 - A / A_h where A is the polygon area of the cloud feature, and A_h is the area of the convex hull containing the polygon. The SCI is closer to 0 for convex polygons (those that do not contain concavities) and SCI approaches 1 as the shape of the polygon becomes complex. A feature that has an SCI > 0.5 for 50% of lifetime is filtered out (see *Section 2.1*).

		Original	This study (*modified from* Maphugwi, 2026)	Brightness Temp. Only
MCS Identification	**Core Cloud Tb** *(K)*	225	**221**	221
	Cold Cloud Tb *(K)*	241	**235**	235
	Minimum Area *(km^2)*	40,000	40,000	40,000
	Minimum Duration *(hours)*	4	4	4
	Minimum PF rain rate *($mm.h^{-1}$)*	2	2	None
	Heavy PF rain rate *($mm.h^{-1}$)*	10	**None**	None
	Shape Complexity Index (SCI)**	No	**Yes**	Yes
MCS Statistics	**Total MCS Count**	804	622	849
	Mean (Std.Dev) Count	57.4 (11.1)	47.3 (6.8)	60.6 (12.6)
	Min. / Max. Count	42 / 74	36 / 61	39 / 82
	Mean % Cont. Rain	40.5	30.1	30.3
	Median % Cont. Rain	40.7	29.5	29.7
	10th / 90th % Cont. Rain	24.8 / 55.6	14.5 / 46.3	15.6 / 45.5
	Mean. % Cont. Light.	55.4	45.1	45.7
	Median % Cont. Light.	55.5	44.5	43.9
	10th / 90th % Cont. Light.	13.4 / 91.6	7.1 / 84.5	7.2 / 84.9

region in southern Africa, this part of the region appears to have an increase (decrease) in MCS frequency during El Niño (La Niña). It is not obvious as to why this may be the case and warrants further investigation. It does highlight the potential mitigating role the Agulhas Current, through large heat fluxes and moisture supply, has on local climate during ENSO events. Thus, could also partly explain why when compared to the rest of eastern southern Africa, the general relationship between ENSO and summer rainfall over parts of eastern South Africa is extremely weak and inconsistent.

This study has also shown that MCSs are not only important rainfall contributors to southern Africa but are also strongly linked to much of the cloud-to-ground lightning activity. In fact, this study is the first of its kind for southern Africa where lightning activity is attributed to a particular type of weather system. The importance of including lightning in the analysis is that many of the regions discussed here contain a large rural population, which are often vulnerable to lightning strikes. It is not just the potential injury and death linked to lightning, but also the economic impacts. Parts of the Mpumalanga and KwaZulu-Natal provinces in South Africa contain large areas of commercial forestry, which would be susceptible to fire through frequent lightning activity.

It was found here that MCSs account, on average, for 20% or more of the summer cloud-to-ground lightning activity for most of the provinces across central and eastern South Africa. This percentage contribution is much higher in northern KwaZulu-Natal, eastern Mpumalanga and northeastern Limpopo, where MCSs account for more than half (≥50%) the summer lightning activity. However, the largest contribution is found over southern Mozambique, with MCSs contributing on average over 60% of the lightning activity in this region. It does need to be considered that the SALDN detection efficiency and location accuracy does deteriorate farther away from the sensors that are based predominantly in South Africa (Gijben, 2012). Although there is relatively good coverage (detection efficiency exceeding 70%) for the neighbouring countries, the SALDN is optimised for South Africa (detection efficiency >90% and location accuracy <0.5 km). Thus, the calculated MCS lightning contribution farther away from South Africa could be biased based on the reduced detection efficiency.

Given the strong links between MCSs and lightning activity, it highlights the need for a better understanding of these systems in southern Africa. For example, it is not clear if the large contribution of MCSs to summer lightning frequency is related to the intensity of the systems, their duration or a combination of both. Although lightning is physically linked to high vertical velocities and ice phase clouds, the role of convective organisation and duration also plays a key role. For comparison, lightning frequency in subtropical South America is associated strongly with both storms having either deep convective cores or wide convective cores (i.e. strong convective systems organising onto the mesoscale; Rasmussen et al., 2014). Lightning frequency over the ocean has been linked to convection having enough time to organise and upscale into an MCS (Bang and Zipser, 2015). This then produces sufficiently strong enough updrafts to develop graupel and supercooled liquid water that can then initiate lightning. Therefore, it is perhaps not surprising to see that the highest lightning contribution from MCSs occurs at the hotspot in MCS 'hours' along the northeast coast of South Africa, southern Mozambique and eSwatini.

There is also some sensitivity in which the contributions are calculated due to the subjectivity in identification and tracking of MCSs. This has been highlighted here by comparing the rainfall contribution determined using the original PyFLEXTRKR settings to that of a modified version applied here. The original PyFLEXTRKR has a much larger rainfall (>40%) and lightning (>80%) contribution by MCS over eastern southern Africa and particularly over the adjacent ocean. As suggested by Maphugwi (2026), the original settings appeared to include many cold front systems that contained similar signatures (i.e., cold cloud tops, large, long lived and embedded heavy rainfall) as MCSs and hence, were included in the tracking methodology. Thus, the original setting may have over emphasised the contribution of MCSs to eastern southern Africa rainfall and lightning activity. This also highlights the importance of adjusting tracking thresholds to the regional climate before building an MCS climatology.

Lastly, a large part of this work has revolved around better

understanding the spatial and temporal patterns of convective activity in southern Africa. Results here confirm that MCSs are an important feature in the regional convective landscape by being a key producer of both lightning and rainfall. It has built on earlier studies investigating convective activity in South Africa through other phenomena such as general lightning activity (Gijben, 2012), hail (Dyson et al., 2020) or severe storm environments (Blamey et al., 2016). Various factors are thought to play a role in this spatial distribution in convective storms, from regional circulation interacting with local topography, through to proximity to the high moisture and latent heat release related to the Agulhas Current. The results have also highlighted the strong seasonal cycle in convection whereby the early summer months tend to be more favourable for large, organised convective systems to develop compared to the late summer months. There are a few key components of southern Africa climate that are not well understood, such as the drivers behind the seasonality seen in MCS activity (or convective activity in general) or large-scale / regional conditions that lead to isolated MCS development versus widespread convective outbreaks. These will be important research avenues to consider going forward given that southern Africa remains not only a water stressed region dependent on these convective storms for rainfall, but a region with a population highly vulnerable to extreme weather events.

CRediT authorship contribution statement

Ross C. Blamey: Writing – review & editing, Writing – original draft, Visualization, Methodology, Investigation, Funding acquisition, Formal analysis, Conceptualization. **Mulalo Maphugwi:** Writing – review & editing, Visualization, Methodology, Data curation. **Cornelia Klein:** Writing – review & editing, Methodology, Formal analysis. **Morne Gijben:** Writing – review & editing, Data curation. **Chris J.C. Reason:** Writing – review & editing, Supervision, Resources, Project administration.

Declaration of competing interest

The authors declare the following financial interests/personal relationships which may be considered as potential competing interests:

Ross Blamey reports financial support was provided by European Union. If there are other authors, they declare that they have no known competing financial interests or personal relationships that could have appeared to influence the work reported in this paper.

Acknowledgements

This publication is part of the EERIE project funded by the European Union (grant agreement ID 101081383). Views and opinions expressed are however those of the author(s) only and do not necessarily reflect those of the European Union or the European Climate Infrastructure and Environment Executive Agency (CINEA). Neither the European Union nor the granting authority can be held responsible for them. CK acknowledges funding from the NERC independent research fellowship "Continental convective organisation and rainfall intensification in a warming world: improving storm predictions from hours to decades" (COCOON; NE/X017419/1). We thank SAWS for making the SALDN data available and NASA for making the IMERG and IR data available for this research. We also thank the reviewers for the insightful comments that have improved the study.

Appendix A. Supplementary data

Supplementary data to this article can be found online at https://doi.org/10.1016/j.atmosres.2026.109156.

Data availability

IMERG precipitation dataset (Huffman et al., 2023) can be retrieved from https://gpm.nasa.gov/data/directory. The dataset of National Aeronautics and Space Administration (NASA) Global Merged IR V1 infrared brightness temperature can be accessed at Janowiak et al. (2017). The SAWS SALDN data is not a publicly available dataset and interested parties should contact SAWS directly. The Python FLEXible object TRacKeR (PyFLEXTRKR) tracking codes (Feng et al., 2021) are available on GitHub (https://github.com/FlexTRKR/PyFLEXTRKR). The MUR SST data (Chin et al., 2017) used in Fig. 1b were provided by JPL under support by NASA MEaSUREs program and is available at http://podaac.jpl.nasa.gov/ws/metadata/dataset/?format=iso&shortName=MUR-JPL-L4-GLOB-v04.1.

References

Ambrizzi, T., Rehbein, A., 2025. South America mesoscale convective systems. In: Oxford Research Encyclopedia of Climate Science. Retrieved 14 Oct. 2025, from. https://oxfordre.com/climatescience/view/10.1093/acrefore/9780190228620.001.0001/acrefore-9780190228620-e-959.

Amell, A., Hee, L., Pfreundschuh, S., Eriksson, P., 2025. Probabilistic near-real-time retrievals of rain over Africa using deep learning. J. Geophys. Res. Atmos. 130, e2025JD044595. https://doi.org/10.1029/2025JD044595.

Andrews, P.C., Cook, K.H., Vizy, E.K., 2024. Mesoscale convective systems in the Congo Basin: seasonality, regionality, and diurnal cycles. Clim. Dyn. 62, 609–630. https://doi.org/10.1007/s00382-023-06903-7.

Asfaw, A., Simane, B., Hassen, A., Bantider, A., 2018. Variability and time series trend analysis of rainfall and temperature in northcentral Ethiopia: a case study in Woleka sub-basin. Weather Clim. Extrem 19, 29–41.

Bang, S.D., Zipser, E.J., 2015. Differences in size spectra of electrified storms over land and ocean. Geophys. Res. Lett. 42 (16), 6844–6851.

Bang, S.D., Zipser, E.J., 2016. Seeking reasons for the differences in size spectra of electrified storms over land and ocean. J. Geophys. Res. Atmos. 121, 9048–9068. https://doi.org/10.1002/2016JD025150.

Blamey, R.C., Reason, C.J.C., 2009. Numerical simulation of a mesoscale convective system over the east coast of South Africa. Tellus A 61 (1), 17–34. https://doi.org/10.1111/j.1600-0870.2007.00366.x.

Blamey, R.C., Reason, C.J.C., 2012. Mesoscale convective complexes over southern Africa. J. Clim. 25 (2), 753–766. https://doi.org/10.1175/JCLI-D-10-05013.1.

Blamey, R.C., Reason, C.J.C., 2013. The role of mesoscale convective complexes in southern Africa summer rainfall. J. Clim. 26 (5), 1654–1668. https://doi.org/10.1175/JCLI-D-12-00239.1.

Blamey, R.C., Reason, C.J.C., 2023. Diversity and ranking of ENSO impacts along the eastern seaboard of subtropical southern Africa. Atmosphere 14 (6), 1042. https://doi.org/10.3390/atmos14061042.

Blamey, R.C., Middleton, C., Lennard, C., Reason, C.J.C., 2016. A climatology of potential severe convective environments across South Africa. Clim. Dyn. 49 (5–6), 2161–2178. https://doi.org/10.1007/s00382-016-3434-7.

Brooks, H.E., Lee, J.W., Craven, J.P., 2003. The spatial distribution of severe thunderstorm and tornado environments from global reanalysis data. Atmos. Res. 67, 73–94. https://doi.org/10.1016/S0169-8095(03)00045-0.

Chen, D., Dai, A., Hall, A., 2021. The convective-to-total precipitation ratio and the "drizzling" bias in climate models. J. Geophys. Res. Atmos. 126, e2020JD034198. https://doi.org/10.1029/2020JD034198.

Chin, T.M., Vazquez-Cuervo, J., Armstrong, E.M., 2017. A multi-scale high-resolution analysis of global sea surface temperature. Remote Sens. Environ. 200, 154–169. https://doi.org/10.1016/j.rse.2017.07.029.

Collins, N., Theurich, G., DeLuca, C., Suarez, M., Trayanov, A., Balaji, V., Li, P., Yang, W., Hill, C., Da Silva, A., 2005. Design and implementation of components in the Earth System Modeling Framework. Int. J. High Perform. Appl 19 (3), 341–350. https://doi.org/10.1177/1094342005056120.

Crook, Julia, Klein, C., Folwell, S., et al., 2019. Assessment of the representation of West African storm lifecycles in convection-permitting simulations. Earth Space Sci. 6 (5), 818–835. https://doi.org/10.1029/2018EA000491.

De Kock, W.M., Blamey, R.C., Reason, C.J.C., 2021. Large summer rainfall events and their potential importance in mitigating droughts over the South Western Cape, South Africa. J. Hydrometeorol. https://doi.org/10.1175/JHM-D-20-0123.1.

Durkee, J.D., Mote, T.L., Sheppard, J.M., 2009. The contribution of mesoscale convective complexes to rainfall across South America. J. Clim. 22, 4590–4605.

Dyson, L.L., Pienaar, N., Smit, A., Kijko, A., 2020. An ERA-Interim HAILCAST hail climatology for southern Africa. Int. J. Climatol. 41 (1), 262–277. https://doi.org/10.1002/joc.6619.

Essa, Y.H., Hunt, G.P., Gijben, M., Ajoodha, R., 2022. Deep learning prediction of thunderstorm severity using remote sensing weather data. In: IEEE Journal of Selected Topics in Applied Earth Observations and Remote Sensing, 15, pp. 4004–4013. https://doi.org/10.1109/jstars.2022.3172785.

Favre, A., Hewitson, B., Tadross, M., Lennard, C., Cerezo Mota, R., 2012. Relationships between cut-off lows and the semiannual and southern oscillations. Clim. Dyn. 38 (1473), 1487. https://doi.org/10.1007/s00382-011-1030-4.

Feng, Z., Houze Jr., R.A., Leung, L.R., Song, F., Hardin, J.C., Wang, J., Gustafson Jr., W.I., Homeyer, C.R., 2019. Spatiotemporal characteristics and large-scale environments of mesoscale convective systems east of the Rocky Mountains. J. Clim. 32 (21), 7303–7328. https://doi.org/10.1175/JCLI-D-19-0137.1.

Feng, Z., Leung, L.R., Liu, N., Wang, J., Houze Jr., R.A., Li, J., Hardin, J.C., Chen, D., Guo, J., 2021. A global high-resolution mesoscale convective system database using satellite-derived cloud tops, surface precipitation, and tracking. J. Geophys. Res. Atmos. 126 (8). https://doi.org/10.1029/2020JD034202 p.e2020JD034202.

Feng, Z., Hardin, J., Barnes, H.C., Li, J., Leung, L.R., Varble, A., Zhang, Z., 2023a. PyFLEXTRKR: a flexible feature tracking Python software for convective cloud analysis. GMD 16 (10), 2753–2776. https://doi.org/10.5194/gmd-16-2753-2023.

Feng, Z., Leung, L.R., Hardin, J., Terai, C.R., Song, F., Caldwell, P., 2023b. Mesoscale convective systems in DYAMOND global convection-permitting simulations. Geophys. Res. Lett. 50 (4). https://doi.org/10.1029/2022GL102603 p. e2022GL102603.

Feng, Zhe, Prein, Andreas F., Kukulies, Julia, et al., 2025. Mesoscale Convective Systems Tracking Method Intercomparison (MCSMIP): Application to DYAMOND global km-scale simulations. J. Geophys. Res. Atmos. 130 (8), e2024JD042204. https://doi.org/10.1029/2024JD042204.

Fensham, H., Hunt, H.G.P., Schumann, C., Warner, T.A., Gijben, M., 2023. The Johannesburg Lightning Research Laboratory—Part 3: Evaluation of the south African lightning detection network. Electr. Power Syst. Res. 216. https://doi.org/10.1016/j.epsr.2022.108968.

Fritsch, J.M., Kane, R.J., Chelius, C.R., 1986. The contribution of mesoscale convective weather systems to the warm-season precipitation in the United States. J. Clim. Appl. Meteorol. 25 (10), 1333–1345. https://doi.org/10.1175/1520-0450(1986)025<1333:TCOMCW>2.0.CO;2.

Funk, C., Peterson, P., Landsfeld, M., Pedreros, D., Verdin, J., Shukla, S., Husak, G., Rowland, J., Harrison, L., Hoell, A., Michaelsen, J., 2015. The climate hazards infrared precipitation with stations—a new environmental record for monitoring extremes. Sci. Data 2 (1), 1–21. https://doi.org/10.1038/sdata.2015.66.

Gahtan, J., Knapp, K.R., Schreck, C.J., Diamond, H.J., Kossin, J.P., Kruk, M.C., 2024. International Best Track Archive for Climate Stewardship (IBTrACS), Version 4r01. Subset - ibtracs.since1980.list.v04r01. NOAA National Centers for Environmental Information doi:10.25921/82ty-9e16. Access date: March 2025.

Garstang, M., Kelbe, B.E., Emmitt, G.D., London, W.B., 1987. Generation of convective storms over the escarpment of northeastern South Africa. Mon. Weather Rev. 115 (2), 429–443. https://doi.org/10.1175/1520-0493(1987)115<0429:GOCSOT>2.0.CO;2.

Gijben, M., 2012. The lightning climatology of South Africa. S. Afr. J. Sci. 108 (3/4). https://doi.org/10.4102/sajs.v108i3/4.740.

Gijben, M., De Coning, E., 2017. Using satellite and lightning data to track rapidly developing thunderstorms in data sparse regions. Atmosphere 8 (4), 67. https://doi.org/10.3390/atmos8040067.

Gill, T., 2008. Initial steps in the development of a comprehensive lightning climatology of South Africa. M.Sc. Thesis. University of the Witwatersrand, Johannesburg.

Harrison, M.S.J., 1984. A generalized classification of South African rain-bearing synoptic systems. J. Climatol. 4, 547–560. https://doi.org/10.1002/joc.3370040510.

Hart, N.C., Reason, C.J.C., Fauchereau, N., 2013. Cloud bands over southern Africa: Seasonality, contribution to rainfall variability and modulation by the MJO. Clim. Dyn. 41, 1199–1212. https://doi.org/10.1007/s00382-012-1589-4.

Hart, N.C., Washington, R., Maidment, R.I., 2019. Deep convection over Africa: annual cycle, ENSO, and trends in the hotspots. J. Clim. 32 (24), 8791–8811. https://doi.org/10.1175/JCLI-D-19-0274.1.

Heikenfeld, M., Marinescu, P.J., Christensen, M., Watson-Parris, D., Senf, F., van den Heever, S.C., Stier, P., 2019. tobac 1.2: towards a flexible framework for tracking and analysis of clouds in diverse datasets. GMD 12 (11), 4551–4570. https://doi.org/10.5194/gmd-12-4551-2019.

Hersbach, H., Bell, B., Berrisford, P., Hirahara, S., Horányi, A., Muñoz-Sabater, J., Nicolas, J., Peubey, C., Radu, R., Schepers, D., Simmons, A., 2020. The ERA5 global reanalysis. Q. J. R. Meteorol. Soc. 146 (730), 1999–2049. https://doi.org/10.1002/qj.3803.

Holle, R.L., 2008. Annual rates of lightning fatalities by country. In: 20th international lightning detection conference. Tucson, Arizona.

Houze Jr., R.A., 2004. Mesoscale convective systems. Rev. Geophys. 42 (4). https://doi.org/10.1002/joc.725.

Houze Jr., R.A., 2018. 100 years of research on mesoscale convective systems. Meteorol. Monogr. 59. https://doi.org/10.1175/AMSMONOGRAPHS-D-18-0001.1 pp.17-1.

Hu, H., Feng, Z., Leung, L.R., Marquis, J., 2025. Examining clustered MCSs and their precipitation significance over global land MCS hotspots. Geophys. Res. Lett. 52 (16), e2025GL114713. https://doi.org/10.1029/2025GL114713.

Huffman, G.J., Coauthors, 2023. IMERG V07 Release Notes, 11 pp. https://gpm.nasa.gov/sites/default/files/2023-07/IMERG_V07_ReleaseNotes_final_230713.pdf.

Huffman, G.J., Tan, J., 2023. The climate data guide: IMERG precipitation algorithm and the Global Precipitation Measurement (GPM) mission. NCAR accessed 12 March 2024. https://climatedataguide.ucar.edu/climate-data/gpm-global-precipitation-measurement-mission.

Huffman, G.J., Bolvin, D.T., Braithwaite, D., Hsu, K.L., Joyce, R.J., Kidd, C., Nelkin, E.J., Sorooshian, S., Stocker, E.F., Tan, J., Wolff, D.B., 2020. Integrated multi-satellite retrievals for the global precipitation measurement (GPM) mission (IMERG). Satell. Precipitation Meas. 1, 343–353. https://doi.org/10.1007/978-3-030-24568-9_19.

Janowiak, J., Joyce, B., Xie, P., 2017. NCEP/CPC L3 half hourly 4 km global (60°S–60°N) merged IR V1. https://doi.org/10.5067/P4HZB9N27EKU.

Kawanishi, T., Coauthors, 2000. TRMM precipitation radar. Adv. Space Res. 25, 969–972. https://doi.org/10.1016/S0273-1177(99)00932-1.

Kekana, B., Blamey, R.C., Reason, C.J.C., 2025. Variability in summer rainfall and rain days over the Southern Kalahari: Influences of ENSO and the Botswana High. Atmosphere 16 (6), 747. https://doi.org/10.3390/atmos16060747.

Knapp, K.R., Kruk, M.C., Levinson, D.H., Diamond, H.J., Neumann, C.J., 2010. The international best track archive for climate stewardship (IBTrACS) unifying tropical cyclone data. BAMS 91 (3), 363–376. https://doi.org/10.1175/2009BAMS2755.1.

Lovie, P., 2005. Coefficient of Variation. In Encyclopedia of Statistics in Behavioral Science (eds B.S. Everitt and D.C. Howell). https://doi.org/10.1002/0470013192.bsa107.

Machado, L., Rossow, W., Guedes, R., Walker, A., 1998. Life cycle variations of mesoscale convective systems over the Americas. Mon. Weather Rev. 126 (6), 1630–1654. https://doi.org/10.1175/1520-0493(1998)126<1630:lcvomc>2.0.co;2.

Malan, N., Reason, C.J.C., Loveday, B.R., 2013. Variability in tropical cyclone heat potential over the Southwest Indian Ocean. J. Geophys. Res. Oceans 118 (12), 6734–6746. https://doi.org/10.1002/2013JC008958.

Malherbe, J., Engelbrecht, F.A., Landman, W.A., Engelbrecht, C.J., 2012. Tropical systems from the Southwest Indian Ocean making landfall over the Limpopo River Basin, southern Africa: a historical perspective. Int. J. Climatol. 32, 1018–1032.

Maphugwi, M., 2026. A Climatology of Mesoscale Convective Systems over Southern Africa. PhD Thesis. In Prep.

Mathon, V., Laurent, H., 2001. Life cycle of Sahelian mesoscale convective cloud systems. Quart. J. Roy. Meteor. Soc. 127, 377–406. https://doi.org/10.1002/qj.49712757208.

Mavume, A.F., Rydberg, L., Rouault, M., Lutjeharms, J.R., 2009. Climatology and landfall of tropical cyclones in the south-west Indian Ocean. West Indian Ocean J Mar Sci. https://doi.org/10.4314/wiojms.v8i1.56672.

Mawren, D., Blamey, R.C., Hermes, J., Reason, C.J.C., 2023. On the importance of the Mozambique Channel for the climate of southeastern Africa. Clim. Dyn. https://doi.org/10.1007/s00382-022-06334-w.

McCain, N., 2022. 'SA sees 100 deaths from lightning strikes a year - now scientists are lobbying for more awareness', *News24*, 29 June. Available at: https://www.news24.com/southafrica/news/sa-sees-100-deaths-from-lightning-strikes-a-year-now-scientists-are-lobbying-for-more-awareness-20220629. Accessed 18 November 2025.

Morake, D.M., Blamey, R.C., Reason, C.J.C., 2021. Long-lived mesoscale convective systems over eastern South Africa. J. Clim. 34 (15), 6421–6439. https://doi.org/10.1175/JCLI-D-20-0851.1.

Mpheshea, L.E., Blamey, R.C., Reason, C.J.C., 2025. The influence of ENSO-type on rainfall characteristics over southern Africa during the austral summer. Clim. Dyn. 63 (3), 161. https://doi.org/10.1007/s00382-024-07489-4.

Mpungose, N., Thoithi, W., Blamey, R.C., Reason, C.J.C., 2022. Extreme rainfall events in southeastern Africa during the summer. Theor. Appl. Climatol. 150 (1), 185–201. https://doi.org/10.1007/s00704-022-04162-w.

Munday, C., Washington, R., 2017. Circulation controls on southern African precipitation in coupled models: the role of the Angola Low. J. Geophys. Res. Atmos. 122, 861–877. https://doi.org/10.1002/2016JD025736.

Ndarana, T., Mpati, S., Bopape, M.-J., Engelbrecht, F., Chikoore, H., 2020. The flow and moisture fluxes associated with ridging South Atlantic Ocean anticyclones during the subtropical southern African summer. Int. J. Climatol. 41. https://doi.org/10.1002/joc.6745.

Prein, A.F., Mooney, P.A., Done, J.M., 2023. The multi-scale interactions of atmospheric phenomenon in mean and extreme precipitation. Earth's Future 11 (11), e2023EF003534. https://doi.org/10.1029/2023ef003534.

Price, C.G., 2013. Lightning applications in weather and climate research. Surv. Geophys. 34 (6), 755–767. https://doi.org/10.1007/s10712-012-9218-7.

Rajagopal, M., Russell, J., Skok, G., Zipser, E., 2023. Tracking mesoscale convective systems in IMERG and regional variability of their properties in the tropics. J. Geophys. Res. Atmos. 128 (24), e2023JD038563. https://doi.org/10.1029/2023JD038563.

Rasmussen, K.L., Zuluaga, M.D., Houze Jr., R.A., 2014. Severe convection and lightning in subtropical South America. Geophys. Res. Lett. 41 (20), 7359–7366. https://doi.org/10.1002/2014GL061767.

Re, Gallager, 2025. Q3 2025 Natural Catastrophe and Climate Report: Preliminary Overview. pg 1–40. https://www.ajg.com/gallagherre/-/media/files/gallagher/gallagherre/news-and-insights/2025/october/natural-catastrophe-and-climate-report-q3-2025.pdf.

Reason, C.J.C., 2001. Evidence for the influence of the Agulhas current on regional atmospheric circulation patterns. J. Clim. 14, 2769–2778. https://doi.org/10.1175/1520-0442(2001)014,2769: EFTIOT.2.0.CO;2.

Reason, C.J.C., Keibel, A., 2004. Tropical Cyclone Eline and its unusual penetration and impacts over the southern African mainland. Wea Forecast. 19, 789–805.

Roca, R., Fiolleau, T., 2020. Extreme precipitation in the tropics is closely associated with long-lived convective systems. Commun. Earth Environ. 1 (1), 18. https://doi.org/10.1038/s43247-020-00015-4.

Rouault, M., White, S.A., Reason, C.J.C., Lutjeharms, J.R.E., Jobard, I., 2002. Ocean–atmosphere interaction in the Agulhas current region and a South African extreme weather event. Wea. Forecasting 17, 655–669. https://doi.org/10.1175/1520 0434(2002)017,0655:OAIITA.2.0.CO;2.

Schumacher, C., Funk, A., 2023. Assessing convective-stratiform precipitation regimes in the tropics and extratropics with the GPM satellite radar. Geophys. Res. Lett. 50, e2023GL102786. https://doi.org/10.1029/2023GL102786.

Schumacher, C., Houze Jr., R.A., 2003. Stratiform rain in the tropics as seen by the TRMM Precipitation Radar. J. Climate 16, 1739–1756. https://doi.org/10.1175/1520-0442(2003)016<1739:SRITTA>2.0.CO;2.

Simpson, L., 2013. Comparing Lightning Polarity and Cloud Microphysical Properties over Regions of High Ground Flash Density in South Africa, 118. University of Pretoria. http://hdl.handle.net/2263/33179.

Sokolowsky, G.A., Freeman, S.W., Jones, W.K., Kukulies, J., Senf, F., Marinescu, P.J., et al., 2023. *tobac* v1.5: introducing fast 3D tracking, splits and mergers, and other enhancements for identifying and analysing meteorological phenomena. EGUsphere 2023, 1–37. https://doi.org/10.5194/egusphere-2023-1722.

Thoithi, W., Blamey, R.C., Reason, C.J.C., 2023. April 2022 Floods over East Coast South Africa: Interactions between a mesoscale convective system and a coastal meso-low. Atmosphere 14 (1), 78. https://doi.org/10.3390/atmos14010078.

Thoithi, W., Blamey, R.C., Reason, C.J.C., 2025. La Niña impacts on Southeastern African climate: the influence of event duration. Int. J. Climatol. 45 (15), e70099. https://doi.org/10.1002/joc.70099.

TimesLIVE, 2020. Three people struck dead by lightning in KZN, bringing the number to 8 in two weeks. In: TimesLIVE, 24 December 2020. Available at: https://www.timeslive.co.za/news/south-africa/2020-12-24-three-people-struck-dead-by-lightning-in-kzn-bringing-the-number-to-8-in-two-weeks/ (Accessed: 18 November 2025).

Tyson, P.D., Preston-Whyte, R.A., 2000. The Weather and Climate of Southern Africa, 2nd ed. Oxford University Press, p. 396. https://doi.org/10.1002/joc.725.

Van Schalkwyk, L., Blamey, R.C., Gijben, M., Reason, C.J.C., 2023. A climatology of dryline-related convection on the western plateau of subtropical southern Africa. J. Geophys. Res. Atmos. 128 (2023), e2023JD038966. https://doi.org/10.1029/2023JD038966Van.

Van Schalkwyk, L., Blamey, R.C., Reason, C.J.C., 2024. The role of drylines in thunderstorm initiation and record rainfall during an anomalously convective early summer season in South Africa. Atmos. Res. 299, 107171. ISSN 0169-8095. https://doi.org/10.1016/j.atmosres.2023.107171.

Van Schalkwyk, L., Blamey, R.C., Munday, C., Washington, R., Reason, C.J.C., 2025. Observations of a dryline interacting with a back-building mesoscale convective system in the Kalahari region of southern Africa. Atmos. Res. 33. https://doi.org/10.1016/j.atmosres.2025.108694.

Vila, D.A., Machado, L.A.T., Laurent, H., Velasco, I., 2008. Forecast and Tracking the Evolution of Cloud Clusters (ForTraCC) using satellite infrared imagery: Methodology and validation. Wea. For. 23 (2), 233–245. https://doi.org/10.1175/2007waf2006121.1.

Yuan, J., Houze, R.A., 2010. Global variability of mesoscale convective system anvil structure from a-train satellite data. J. Clim. 23 (21), 5864–5888. https://doi.org/10.1175/2010JCLI3671.1.

Zipser, E.J., Cecil, D.J., Liu, C., Nesbitt, S.W., Yorty, D.P., 2006. Where are the most intense thunderstorms on Earth? BAMS 87 (8), 1057–1072. https://doi.org/10.1175/BAMS-87-8-1057.